Biophysical analysis of the interaction of laminin-related protein Netrin with its receptor Neogenin

Shubleen Sidhu

University of Manitoba

A Thesis submitted to the Faculty of Graduate Studies in partial

fulfillment of the requirements of the degree of

Master of Science

Department of Chemistry

University of Manitoba

Winnipeg, Manitoba, Canada

Abstract

Netrins are axon guidance cue molecules belonging to the laminin related protein. These molecules play a significant role in neuronal migration, by releasing chemotrophic cues and allowing either chemoattraction or chemorepulsion. Netrin holds capability to bind multiple different receptors including Deleted in Colorectal Cancer (DCC), Uncoordinated 5 (UNC5) and Neogenin (Neo). In order to investigate the binding of Netrin with its receptor Neogenin, two different constructs of Neogenin, Neogenin 3-5 Long and Neogenin 3-5 Short were investigated with its binding partner Netrin in a biophysical approach followed by crystallization screening. Netrin and the two constructs of Neogenin alone and in complex were analysed by gel electrophoresis, Size exclusion chromatography, dynamic light scattering (DLS) and small angle X-ray scattering (SAXS). The findings from the low-resolution models reveal that the models for the complex appear larger and more compact than the individual models of the chNet△C, Neogenin Long 3-5 and Neogenin Short 3-5, which appear elongated. The models propose the following D_{max} values which indicate complex formation, D_{max} = for 198.1nm chNet△C, D_{max} = 162.3nm for Neo Long 3-5, D_{max} = 157.8nm for Neo Short 3-5 D_{max} = 240.9nm for chNet△C-Neo Long 3-5 complex and D_{max} = 252.0nm for chNet△C- Neo Short 3-5 complex. This analysis provides some insight into the interaction of Netrin with Neogenin and identifies 47% w/v 2-methyl-2,4- pentanediol 100mM HEPES, pH 7.5 and 35% w/v 2-methyl-2,4- pentanediol 100mM Imidazole, pH 8.0 as preliminary conditions for crystallization of the complex.

Acknowledgements

I would like to thank Dr. Jorg Stetefeld, Dr. Markus Meier, Dr. Matthew McDougall and Dr. Aniel Moya for their supervision, guidance and support.

Many thanks also go to Monika Gupta, Haben Gabir and Dr. Natalie Krahn for their friendship, advice and support. In addition, I would like to express my appreciation for financial assistance from the Department of Chemistry, Faculty of Science and Faculty of Graduate Studies at the University of Manitoba.

Table of Contents

List of Tables

List of Figures

1. Introduction

1.1 SIGNIFICANCE OF NETRIN IN THE HUMAN BODY

Netrins are a family of laminin related proteins that act as axon guidance cue molecules (1,2). These molecules serve as bifunctional signals, where they attract some neurons and repel others as the brain develops. Their function is concentration dependent in that a growing axon will either move towards or away from an area of higher concentration of Netrin, allowing Netrin chemotrophic properties (1-3).

The family of netrins includes five mammalian netrins, netrin-1, netrin-3, netrin-4, netrin-5 and the glycosylphosphatidylinositol (GPI)- anchored netrins-G1 and -G2, however, Netrin-1 is of particular interest (4,5). Netrin-1 encoded by the NTN1 gene is known to play various key roles including neuronal navigation, immune cell migration, angiogenesis and cell survival (5). Moreover, Netrin-1 has also been shown to have implications in multiple diseases including diabetes, cancer and cardiovascular diseases (6,7).

Netrin has been extensively researched for its role in many diseases but most importantly for its role in cancer (8). Netrin-1 signalling pathways have been shown to be upregulated in several cancer types including colorectal cancer, non-small cell lung cancer, neuroblastoma, glioblastoma and metastatic breast cancer (8,10). The significance of Netrin in the evolution of tumor comes from its ability to regulate cell proliferation and cell mobility (8,9). Increasing cell proliferation and mobility of cancerous cells allows them to increase in number at a much faster rate and invade other tissues, ultimately allowing a faster spread of cancer (10).

1.2 CRYSTAL STRUCTURE OF NETRIN

The full- length molecule of Netrin is one that consists of 600 amino residues (4). The peptide sequence of Netrin begins with a signal peptide consisting of 24 residues and reveals three asparagine-linked glycosylation sites at Asn95, Asn116 and Asn131 (4). Multiple disulfide bridges throughout the molecule help stabilize the secondary structure of the molecule (11).

The crystal structure of this molecule reveals an N-terminal laminin domain (LN also known as domain VI), followed by three laminin-type epidermal growth factors (LE) repeats (LE1, LE2 and L3; also known as domain V) and as well as a positively charged C-terminal domain (4,11). The crystal structure for mouse Netrin-1 as depicted in Figure 1 was resolved by Dr. Markus Meier at a resolution of 2.64A^{o} and as such shows a head to stalk like arrangement of the molecule, where the globular shaped N terminal domain forms the head (4). The head is followed by three rod- like LE domains that make up the stalk. The three consecutive LE domains with their irregular coil segments allow the molecule an overall linear and elongated appearance (4).

Figure 1. Ribbon Model structure of Netrin-1. The N-terminal LN domain is shown in red along with three LE repeats LE1 (magenta), LE2 (blue), LE3 (yellow). N-linked glycans are drawn as green sticks, and calcium ions as green spheres (PDB: 4OVE).

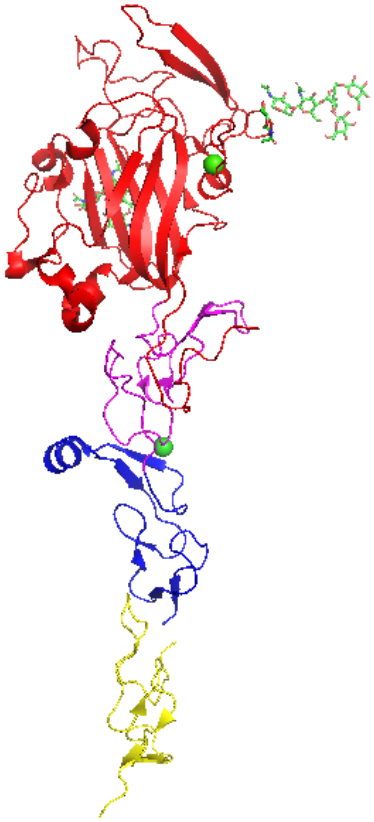

1.3 NETRIN AND ITS RECEPTORS

Netrins are proteins that conduct both attractive and repulsive responses in neurons by extending axons and migrating cells in the central and peripheral nervous system (9,13). They are able to carry out both attractive and repulsive cues due to their ability to bind multiple different receptors (10). This activity of Netrin-1 is regulated through the induction of signal transduction pathways upon binding to receptor. Upon binding different receptors in nanomolar affinity, a signal is transmitted across the membrane of a migrating neural cell, and the appropriate response is brought upon by the cell (9).

This control of neural navigation in the nervous system is accomplished through the binding of Netrin-1 to one of its main receptors deleted in colorectal cancer (DCC) and Uncoordinated 5 (UNC5) (6-11). Another very important but lesser known receptor of Netrin-1 includes Neogenin (11).

The binding of DCC with Netrin-1 results in attractive guidance cues whereas binding of Netrin-1 with UNC5 leads to repulsive cues (12,14). Both DCC and UNC5 are single pass transmembrane receptors, which induce cell death when alone and not interacting with ligands such as Netrin (13). However, in the presence of such ligands, the dependence receptors bind and block the proapoptotic activity of the cells. The binding of Netrin with its receptors activates a signal transduction pathway which brings upon positive signals in the cells that lead to the activation of proteins such as MAPK and PI3K (4). In instances where the receptors are unbound, apoptosis of the cells is triggered.

Netrin-1 associated repulsive cues are brought upon through the interaction of Netrin with its receptor UNC5 (14). Four different orthologues of UNC5 have been identified in mammals including UNC5H1, H2, H3 and H4 (12,16). Recent studies on the interaction of

UNC5H with Netrin-1, reveal UNC5H as another tumor suppressor (15). UNC5H genes were also shown to be downregulated in many cancers, especially colorectal cancer (16).

UNC5 is a transmembrane receptor consisting of both intracellular and extracellular domains (15). The extracellular domain of UNC5 consists of two immunoglobulin repeats and two membrane- proximal thrombospondin repeats (18). The intracellular domain of UNC5 consists of three identified conserved domains: a ZU5 domain, a DCC-binding (DB) domain and a death domain (DD) (19). Axonal repulsion by UNC5 is brought upon as Netrin-1 binds both immunoglobulin repeats.

From all the receptors that can bind Netrin-1, the interaction between DCC and Netrin-1 is the most well researched. DCC, which is known to be a tumor suppressor gene is located on chromosome 18q21 (11). In the absence of Netrin-1, DCC can trigger apoptosis in tumor cells that would otherwise proliferate and cause cancer (14,16). Therefore, the loss of DCC has been implicated in advanced colorectal and many other cancers (17).

DCC is a transmembrane receptor which consists of an extracellular domain and as well an intracellular domain (19). The extracellular domain of DCC consists of four immunoglobulin-like domains and six fibronectin type III (FNIII) domains (11,14). Previous research conducted on the interaction of DCC with Netrin-1, revealed the interaction of the FNIII repeats of DCC with the LN and LE regions of Netrin-1 (14,15). Furthermore, in-vitro studies suggest that the FNIII domains of DCC play a crucial role in bringing upon apoptosis of cancerous cells. Hence upon the binding of Netrin with DCC, these FNIII domains are no longer available to trigger apoptosis (14,17).

The intracellular domain of DCC consists of three domains P1, P2 and P3 (18, 19). These domains hold phosphorylation and binding sites for intracellular proteins but have no known catalytic function (19). The P2 domain is known to be rich in proline residues and contains four PXXP putative SH3 domain-binding motifs (18,19). The P3 domains contains many highly conserved phosphorylation sites (19).

The DCC receptor is required for axon chemoattraction to Netrin-1 (18). As Netrin-1 binds, it induces the multimerization of DCC through the association of the P3 domains, a step that is essential for chemoattraction (20). Phosphatidylinositol transfer protein- α (PITPα) can bind the P3 domain of DCC and promote the production of phosphoinositides (PIPs) by phosphatidylinositol 3-kinases (PI3Ks) (19,20). These PIPs can then by hydrolyzed by phospholipase C (PLC) into inositol 1,3,5- triphosphate (IP3) and diacylglycerol (DAG) which leads to Ca2+ release from the intracellular stores and hence activation of protein Kinase C (PKC) (19). Once Netrin-1 binds to DCC, the intracellular domains of DCC are phosphorylated and that leads to the association of many proteins such as Fak, Fyn and Pak (19). As the intracellular Ca2+ levels increase, Rho GTPases Cdc42 and Rac proteins are activated and cause the remodeling of the cytoskeleton through proteins such as the Wiskott-Aldrich syndrome protein (N-Wasp), Ena/Vasp, and Map1b (19,20,28).

1.4 NEOGENIN BINDS NETRIN ALLOWING IT ATTRACTIVE GUIDANCE CUE PROPERTIES

Another receptor for Netrin-1 is a DCC paralogue Neogenin (11). This attractive guidance cue molecule is one that plays a role in neural development, morphogenesis, cell migration, differentiation and apoptosis (11,20-21,28). Besides Netrin-1, Neogenin can bind Netrin-3 to mediate signalling during myotube-3 formation and as well bind Netrin-4 for signalling during angiogenesis (18). Neogenin mediates axon guidance and controls neural differentiation by either binding Netrin-1 or Repulsive guidance molecule a (RGMa). Upon binding with Netrin-1, Neogenin promotes chemoattraction, and on binding RGMa, it promotes chemorepulsion (22-24). However, prior research suggests Neogenin has a higher affinity for RGMa over Netrin-1 (27).

Neogenin is homologous to DCC in that it shares 50% amino acid identity with DCC and has an identical secondary structure (26). Belonging to the group of dependence receptors Neogenin induces apoptosis in cells in the absence of its ligand (18,25). As such any cancerous cell is able to escape apoptosis in the presence of the ligand Netrin. This further allows cancerous cells to proliferate at a higher rate and spread faster.

Like DCC and Unc5, Neogenin is also a single-membrane spanning protein that consists of both intracellular and extracellular domains (24). It is a member of the Ig superfamily and as depicted in Figure 2a. the intracellular domains consists of four immunoglobulin-like (Ig) domains followed by six fibronectin type III (FNIII) domains (FN1-FN6) and a transmembrane domain (24-26). The intracellular domain similar to that of DCC consist of P1, P2 and P3, which allow intracellular binding of other proteins (19).

Previously, the structure of the netrin/Neogenin complex has been determined at a 3.2A^{o} resolution (11). A Neogenin construct consisting only of domains FN4 and FN5 is known to interact with Netrin as a 2:2 heterotetramer in a head-to-head X-shaped dimer (11). Two molecules of Netrin interact with the FN4 and FN5 domains of two molecules of Neogenin. Here the LN domain of one Netrin interacts with the FN4 domain of Neogenin, while the LE3 domain of the same Netrin interacts with the FN5 domain of another molecule of Neogenin (11). In a similar manner another molecule of Netrin is involved and brings about the 2:2 heterotetramer conformation.

Based on prior research conducted by other groups, for the purpose of our own study, two different constructs of Neogenin were used. These constructs are Neogenin Long 3-5 (Neo Long 3-5) and Neogenin Short 3-5 (Neo Short 3-5). As Figure 2b and c show, these constructs only consist of domains FN3-FN5 and are hence deprived of all other domains that make a full length Neogenin molecule. The Neo Long 3-5 construct consists of a linker sequence composed of 16 amino residues situated between the FN4 and FN5 domains, which is missing in the Neo Short 3-5 construct.

Figure 2. Schematic representation of Neogenin. (A) Domains of Neogenin are labelled starting with Ig, Immunoglobulin domains coloured in sky blue, FN, Fibronectin domains in dark blue, TM, Transmembrane domain in blue and Three P domains in green. (B) Neogenin Short 3-5 construct composed of FN3-5 as shown in dark blue. (C) Neogenin Long 3-5 construct composed of FN3-5 with an additional linker sequence situated between FN4 and FN5.

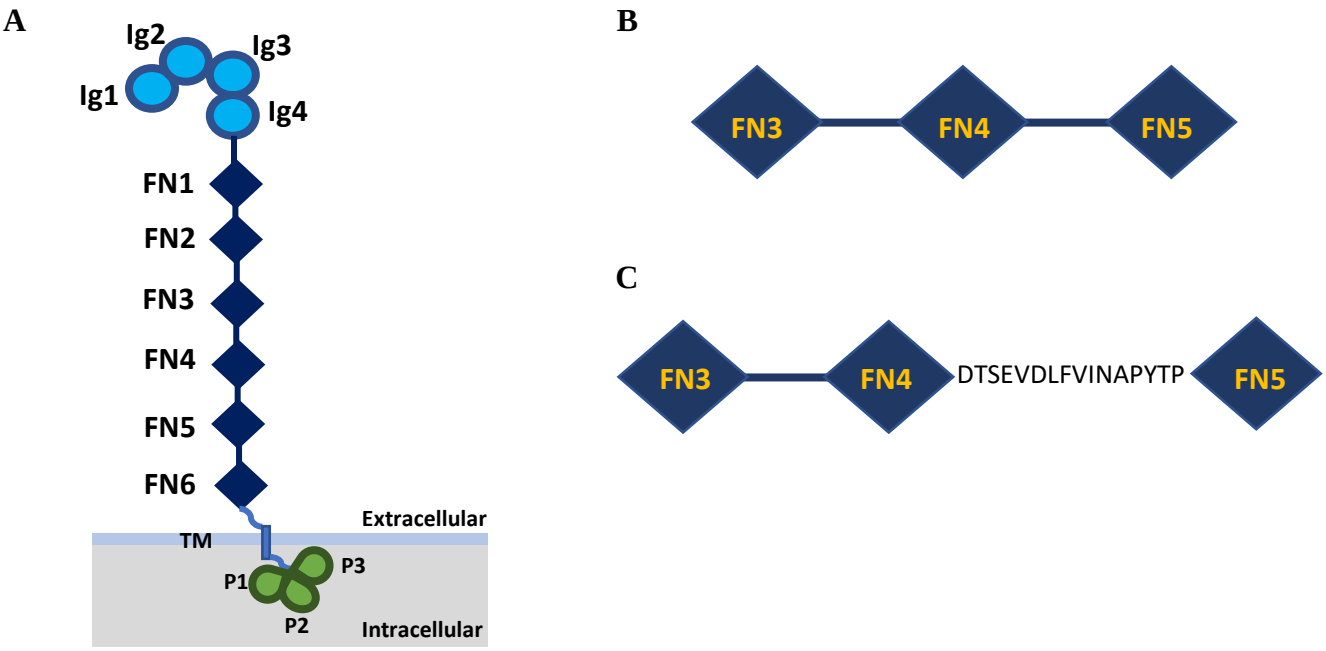

1.5 OBJECTIVES

Here, we investigated the binding of Netrin with two different constructs, Neogenin Long 3-5 and Neogenin Short 3-5. To study the interaction between this ligand and receptor many preliminary steps must be mastered before the use of biophysical approaches. The first goal encompasses, successful protein production through cell proliferation of protein expressing cells. Upon successful protein production, the protein must be successfully purified through strep-Tactin affinity chromatography and Size exclusion chromatography. Successful binding of the ligand and receptor is then required prior to analysis through biophysical techniques, including DLS and SAXS. In addition, for the purpose of X-ray crystallography, several potential conditions for crystallization of the complex were identified. Although structures of the complex between Netrin and Neogenin is available, there is a lack of information as to how other domains of Neogenin interact with a full-length Netrin molecule. This is an important path for investigation as the binding of Netrin with Neogenin promotes chemoattraction and hence cell proliferation by allowing cancerous cells to avoid apoptosis.

2. Materials and Methods

2.1 MAMMALIAN CELL CULTURE

Chicken Netrin-1 gene (*NTN1* GenBank ID Q90922) lacking the c-terminal domain was inserted into HEK293 chromosome to express recombinant protein chNet1△C using sleeping beauty transposon system to obtain stable transfected clones (28). Neogenin gene *Mus musculus* gene *Neo1* (Gen Bank ID P97798) truncated versions (Fibronectin domain 3-5, a.a 667-986) were also stably transfected with sleeping beauty transposon system into HEK293 cells (28). Mouse Neogenin produced in this study only consisted of recombinant Neogenin fragment domain FN3-5, with and without the linker regions referred to as Neo Long 3-5 and Neo Short 3-5 respectively. In the sleeping beauty transposon plasmid used to generate HEK293 clones, in the DNA construct the gene expression was regulated by the TRE promoter inducible by doxycycline (29) and the protein produced had an additional sequence for thrombin cleavage (LVPRGS) followed by two strep-tag peptides in a row at the c-terminal end to facilitate protein purification. Cloning, DNA sequencing and generation of stable cell clones were performed in Professor Manuel Koch Lab at the University of Cologne, Germany and HEK293 cell were sent to our lab for protein production. Upon arrival, cells expressing Netrin-1 and Neogenin1 FN3-5 were transferred to T75 flask containing DMEM, 10% FBS (Thermo Fisher Scientific, Massachusetts, USA) and incubated at 37^{o}C in humidified atmosphere with 5% CO_2. Adherent cells grew until 90% confluency before resuspended in FBS, 10% DMSO and transferred to cryovials and stored in liquid N_2.

2.2 CLONAL SELECTION

HEK293 cell pools were thawed for less than 1 minute at 37°C and transferred to T75 flasks containing 10mL of DMEM, 10% FBS. Culture media was replaced by fresh media after 24 hours to removed death cells and DMSO traces from cryo-media and cells were incubated at 37°C, in humidified atmosphere with 5% CO_2. Once cells were 90% confluent, culture media was aspirated, and cells washed once with 10ml sterile PBS. To detach cells from flask surface, a volume of 3ml of TrypleE (Gibco, Life Technologies, New York, USA) was added to the flask and incubated at 37ºC for 3 minutes. Detached cells were resuspended in DMEM and cell viability determined using Trypan Blue Stain 0.4% (Life Technologies Corporation Oregon, USA) and a Countess IIFL cell counter (Life Technologies Corporation Oregon, USA). Cells were diluted and transferred to a 96-well plate (Corning Incorporated Life Sciences, Massachusetts, USA) ensuring a one cell per well consistency through the 96-well plate. Cells were allowed to grow until they covered >50% of the well surface and protein production was induced in each well by adding DMEM, 1µg/ml Doxycycline. After 24 hours incubation at 37°C, 5% CO2, a volume of 100 µl of supernatant from each selected well was applied to a 96-well Bio-Blot (Bio-Rad) that contained a Nitrocellulose (NC) membrane on each well. The microfiltration apparatus Bio-Blot permits the rapid immobilization of protein samples onto a Nitrocellulose membrane after the application of vacuum (30). A volume of 200 µl of PBS buffer was added to remove removed non bound free protein from NC. Then, NC membrane was removed from the Mio-Blot apparatus and blocked with 1X IBind solution (Thermo Fisher Scientific, Massachusetts, USA). NC membrane was transferred to IBind Western System device (Thermo Fisher Scientific, Massachusetts, USA) to detect the presence of tag protein using a

specific anti Step-tag II monoclonal antibody conjugated to horseradish peroxidase (iba Solutions for Life Sciences, Goettingen, Germany). Luminate Forte HRP substrate (Millipore Sigma, Massachusetts, USA) was added to the membrane to visualize by chemiluminescence the production of secreted strep-tag recombinant protein. Dot blot was imaged using the Cell Biosciences imager (Cell Biosciences, Santa Clara, USA). Intensity of fluorescence corresponded with the amount of protein produced by each clone after 24 hours in the presence of the inducer doxycycline. Higher protein producing clones were selected and used to inoculate 24 well culture plate. Depending on cell viability and protein production cells were further moved down to 12 well plate and eventually to a six well plate. Three of the best clones were chosen and added separately to T75 flasks. Upon confluency, one out of the three clones, was selected and split for further protein production. Selected clone was used to inoculate T75 flasks with 10mL DMEM, 5% FBS, 5µg/ml puromycin. Individual clones were resuspended in 1.5ml cryo-media consisting of 90%FBS and 10% DMSO and then frozen gradually at -20°C for couple hours, then moved to -80°C overnight and finally frozen in liquid nitrogen.

2.3 PROTEIN PRODUCTION IN *HYPERFlask*

Clonal selected clone was expanded in T75 flasks and 95% confluent adherent cells were used to seed a Hyperflask (Corning, Incorporated Life Sciences). Briefly, 1.0×10^7 cells were resuspended in 50 ml of fresh DMEM, 5% FBS. Cells were then equally distributed to all layers of HYPER Flask and 500ml of DMEM, 5% FBS was added, according to Corning Hyperflask specifications (31). Cells were allowed to grow until 90% confluency upon which media was exchanged by the expression media DMEM, 2.5%FBS, 1µg/ml of Doxycycline. Cell culture media containing recombinant protein was collected every 2 days, sterile filtered and stored at -

20ºC until use. Each media collection was followed by the addition of fresh expression media in the Hyperflask. A total of 5 supernatant collections were performed and stored at -20°C until use. All three proteins chNet1△C, Neo Long 3-5 and Neo Short 3-5 were produced in similar ways using a HYPER flask.

2.4 PURIFICATION OF NETRIN/NEOGENIN WITH STREP TACTIN COLUMN

For strep-tagged protein affinity purification, supernatant was adjusted to 20 mM Tris pH 8, 500 mM NaCl with stock solutions 1M Tris HCl, pH 8.0 and 5M NaCl before affinity chromatography purification. To purify Strep tag recombinant proteins, a 5ml StrepTrap HP column prepacked cartridge with StrepTactin sepharose beads was used (GE healthcare, Chicago, Illinois, USA). Strep-tactin column was equilibrated with 5 column volumes of 50mM Tris, pH 8.0 500mM NaCl buffer. Cell culture supernatant was then run through the affinity column. Column was washed with 2 column volumes of 50mM Tris, pH 8.0 500mM NaCl and 3 column volumes of 50mM Tris pH 8.0 1M NaCl. Protein elution was performed with 3 column volumes of 50mM Tris, pH 8.0, 500mM NaCl, 2.5 mM of d-Desthiobiotin. Column was regenerated with 5 column volumes of 100mM Tris, pH 8.0, 150mM NaCl, 1mM EDTA, 1mM HABA, followed by 50 mM Tris, pH 8.0, 500mM NaCl.

2.5 PREPARATION OF NETRIN

2.5.1 *Strep Tag Removal of Netrin*

ChNet1△C- strep-tag eluted was concentrated to 1.0mg/ml in Amicon Ultra 30Kda cut-off centrifugal filter (Millipore Sigma, Ireland). To remove the Strep-tag, thrombin from bovine plasma (GE Healthcare, Chicago, Illinois, USA) was used to a ratio of 1 unit of thrombin per mg

of protein. A dialysis membrane (Spectrum Laboratories Inc. Rancho Dominguez, CA, USA) with cut-off of 6-8kDa was used and protein was dialyzed for 24 hours at room temperature into 500ml of 50mM Tris, pH 8.0, 1M NaCl, 0.15M glycine, 2.5mM $CaCl_2$.

2.5.2 *Separation of tag free Netrin*

Upon overnight dialysis, tagged and untagged chNet1△C was separated using a Strep Tactin column. Column was equilibrated with 5 column volumes of 50mM Tris, pH 8.0, 1M NaCl. Dialyzed protein was applied to the column and untagged protein was collected. Tagged netrin protein bound to the column was eluted by applying 3 column volumes of 50mM Tris, pH 8.0, 1M NaCl, 2.5 mM d-desthiobiotin. Column was regenerated with 5 column volumes of 100mM Tris, pH 8.0, 150mM NaCl, 1mM EDTA, 1mM HABA and 50mM Tris, pH 8.0, 500mM NaCl. To remove thrombin in the tag free recombinant protein a HiTrap Benzamidine column (GE healthcare, Chicago, Illinois, USA) was used. Untagged chNet1△C protein was dialyzed for 24 hours at room temperature in 500ml of 50mM Tris, pH 7.5, 1M NaCl with a buffer change once through the dialysis. Dialyzed protein was stored at 4^{o}C at a concentration of 1mg/ml or less until further use. Strep-tag removal was confirmed by SDS-PAGE and Western-Blot.

2.6 PREPARATION OF NEOGENIN LONG/SHORT

2.6.1 *Strep Tag Removal of Neogenin Long/ Short*

Neo Long 3-5 and Neo Short 3-5 strep-tag proteins were separately added to the dialysis bag (cut-off 6-8 kDa) along with thrombin at a concentration of 1unit of thrombin per mg of protein. Protein was dialyzed for 24 hours at room temperature into 500ml of 50mM Tris, pH 7.5, 200mM NaCl.

2.6.2 *Separation of tag free Neogenin Long/ Short*

Tagged and untagged recombinant proteins were separated using Strep Tactin column. Column was equilibrated with 5 column volumes of 50mM Tris, pH 8.0, 500mM NaCl. Dialyzed protein was applied to the column and untagged protein was collected. Tagged Neogenin protein bound to the column was eluted by applying 3 column volumes of 50mM Tris, pH 8.0, 0.5 mM NaCl, 2.5 mM d-desthiobiotin. Strep-tactin column was regenerated with 5 column volumes of 100mM Tris, pH 8.0, 150mM NaCl, 1mM EDTA, 1mM HABA and 50mM Tris, pH 8.0, 500mM NaCl. To remove thrombin in the tag free recombinant protein a HiTrap Benzamidine column was used. Strep-tag removal was confirmed by SDS-PAGE and Western-Blot.

2.6.3 *Purification through Size Exclusion Chromatography (SEC)*

Protein was purified on a Superdex 200 10/300 GL SEC column equilibrated with 50mM Tris, pH 7.5, 200mM NaCl. A homogenous peak corresponding to a single protein was observed on the Size exclusion chromatogram, and protein fractions were collected according to the absorbance at A_{280}.

2.7 PREPARATION OF PROTEIN COMPLEXES

ChNet1△C and Neo Long/Short purified protein were mixed in 1:1 molar ratio. Each component at a concentration of 110µM was loaded into a dialysis bag and dialyzed for 24 hours at room temperature in 50mM Tris, pH 7.5, 200mM NaCl, with a buffer change once through the dialysis. The complexes formed were purified on a Superdex 200 10/300 GL SEC column equilibrated with 50mM Tris, pH 7.5, 200mM NaCl. Fractions corresponding to protein complex

peak were combined and concentrated. Protein concentration was measured using a Nano Drop microvolume spectrophotometer (Thermo Fisher Scientific, Massachusetts, USA). For Neo Long 3-5 and chNet1△C complex a molecular weight of 86.096kDa and an extinction coefficient of ε_{260}= 106 295 M^{-1} cm^{-1} was used to determine protein concentration. For Neo Short 3-5 and chNet1△C complex a molecular weight of 84.333kDa and an extinction coefficient of ε_{260}= 104 805 M^{-1} cm^{-1} was used to calculate protein concentration. Molecular weights and extinction coefficients were calculated using the ExPASy ProtParam (*Protein Identification and Analysis Tools on the ExPASy Server*) (32).

2.8 POLYACRYLAMIDE GEL ELECTROPHORESIS (SDS PAGE)

Protein samples and molecular weight standard ladder (Percision plus protein ladder, Bio-Rad, CA, USA) were separated using 8% Tricine SDS-PAGE gel electrophoresis, at a constant 10 watts in PowerPac HC (Bio-Rad Laboratories Inc. CA, USA) using SDS-PAGE running buffer (25mM Tris base, 200mM glycine, 0.1% w/v SDS). After electrophoresis the gel was soaked in Coomassie Gel Staining Solution for a few hours before destaining with a Gel Destain solution. Gel was visualized using the Alpha Imager HP system (Alpha Innotech, CA, USA).

2.9 DYNAMIC LIGHT SCATTERING (DLS)

Data were collected using the Nano-S Dynamic Light Scattering system (Malvern Instruments Ltd. Malvern, UK) equipped with a 663nm laser and using 173° scattering angle. All protein solutions were filtered using 0.1μm centrifugal filter (Millipore, USA) and equilibrated to 20°C for 30 minutes prior to data collection. Neo Long alone and protein complexes were measured separately in a 45μL quartz cuvette at a range of concentrations. Protein alone and its

complex were measured in 50mM Trist pH 7.5 200mM NaCl. Measurements were collected in automatic mode and 15 measurements were obtained for each concentration.

2.10 SMALL ANGLE X-RAY SCATTERING (SAXS)

Samples were sent to Diamond Light Source Limited (Chilton, Didcot, Oxfordshire) for BioSAXS data collection with their respective concentrations included, chNet1△C (6.3mg/ml), Neo Short (8.0mg/ml), Neo Long (7.9mg/ml), chNet1△C with Neo Short (9.0mg/ml) and chNet1△C with Neo Long (9.3mg/ml). Data were collected by a beamline scientist with a B21 High Throughput SAXS beamline with beam size <75μm and an Eiger 4M detector (30). B21 beamline operates with a fixed camera length configuration (4.014 meters) at 12.4 KeV. Data collection was through standard data collection method of size- exclusion chromatography coupled SAXS using an Agilent HPLC system with a KW400 series Shodex column. Buffer and sample at a range of concentrations were each exposed from 0.5 seconds to 5 minutes and the raw data was reduced and analyzed using the scatter software. The momentum transfer, s, was defined as follows: $s=4\pi\sin\theta/\lambda$, where θ is the scattering angle and λ is the wavelength (34). Individual data sets were merged and radius of gyration (R_g) and maximum particle dimension (D_{max}) were calculated using the program PRIMUS (35). An algorithm DENSS was used for calculating 3D particle electron densities directly from 1D solution scattering data. Multiple low-resolution solution models were generated by DAMMIF, a rapid ab *initio* shape determination program that relies on simulated annealing using a single-phase dummy atom model (36). Furthermore, a program DAMAVER was used to align these ab *initio* models and build an averaged model.

2.11 CRYSTALLIZATION TRIALS

In an effort to obtain protein crystals for the Netrin-Neo Long and Netrin- Neo Short complexes, crystallization trials were conducted using commercial crystallization kits from Jena Bioscience (Jena, Germany) and Hampton Research (CA, USA). The complexes were prepared as described above in section 2.7. Sitting drops for Netrin-Neo Long 3-5 composed of 0.4µl of the species to be crystallized and 0.4µl of the reservoir solution was set up in 96 well plates using the Arts Robbins Instruments- Crystal Gryphon (Sunnyvale CA, USA). Sitting drops for Netrin-Neo Short 3-5 composed of 0.3µl of the species to be crystallized and 0.3µl of the reservoir solution was set up in 96-well-3 LVR plate (Hampton Research, CA, USA) in the same manner. Each of the wells contained 50µL of reservoir solution. All species were filtered using 0.2µm filters prior to crystallization. The plates were covered and sealed with clear protective film (Clear Seal Film, Hampton Research, CA, USA) and incubated for 20°C. Jena Bioscience Screen 1-4, 5-8, 9-10 and JCSG +++1-4 (Jena, Germany) and Hampton Research screens, Crystal Screen HT, Natrix HT, Index HT and PEG/ION HT (CA, USA) were used to test crystallization conditions for Netrin-NeoShort at 9.3mg/ml. Similarly, Jena Bioscience Screen 1-4, 5-8, and JCSG +++1-4 (Jena, Germany) and Hampton Research screens, Crystal Screen HT, Natrix HT and Index HT (CA, USA) were used to test crystallization conditions for Netrin-Neo Long at 12.4mg/ml. Concentration of the complexes were determined spectrophotometrically using the Nano Drop Microvolume Spectrophotometer and parameters calculated on the basis of equimolar binding between both proteins in a complex. The crystal plates were observed for crystals growth daily for the first week, every three days for the next week, weekly for the subsequent month and monthly for the remainder of the time using the Olympus SZX10 Microscope (Olympus Life Science, Japan, Tokyo).

3. Results

3.1 EXPRESSION AND PURIFICATION OF NEOGENIN SHORT AND NEOGENIN LONG 3-5.

In order to perform biophysical assays on Neogenin and Netrin, expression of Neo Long3-5 and Neo Short 3-5 was performed in HEK293 cells. Neo Long 3-5 and Neo Short 3-5 both only consist of Fibronectin regions 3-5 in an anticipation to improve the ability of the protein to crystallize and to deduce the interaction of these regions with Netrin-1. Cells expressing both constructs of Neogenin were successfully grown to confluency in T75 flasks and moved to a 96 well-plate ensuring a one cell per well consistency. A western Dot Blot was performed by inducing the TRE promoter with doxycycline to quantify the amount of protein produced by each clone through fluorescence **(Figure 3A and 3B).** The intensity of the green fluorescence in each clone, represented by a dot, directly corresponds to the amount of protein produced by the clone and as such, clones with brighter intensity are desired. To ensure the accuracy of the dot blot experiment, a DCC with strep tag was used as a positive control and DCC without strep tag was used as a negative control. The intensity was compared between the clones, and three of the brightest clones were selected for storage, and furthermore, one of the three clones was used to inoculate the hyper flask. Clone D11 was used for Neo Long3-5 hyper flask and clone D2 was used for Neo Short 3-5 hyper flask. A total of 5 supernatant collections were collected and purified using Strep- Tactin columns which resulted in an average of 10mg total of protein from each collection.

Upon retrieval of the protein from the column, both Neo Short and Neo Long 3-5 were dialyzed in 50mM Tris, pH 7.5 200mM NaCl, along with bovine plasma thrombin to cleave off the strep tag. To ensure successful cleavage of the strep tag, both Neo Long 3-5 and Neo Short 3-

5 with and without tag were subjected to analysis through SEC and SDS-PAGE Gel. A slight downward shift on the SDS PAGE gel indicates ~3kDa reduction in protein size which can be attributed to successful strep tag removal **(Figure 4a, 4B and 4C).**

Further analysis to ensure successful cleavage of strep tag was carried out on the Superdex 200 10/300 GL SEC column. For both proteins, samples with and without tag were run on the column in 50mM Tris, pH 7.5 200mM NaCl. The size exclusion chromatogram **(Figure 5)**, shows two peaks, Neo Short 3-5 with tag which elutes at 13.9ml and Neo Short 3-5 without tag which elutes out at 14.3ml. Likewise, two peaks that correspond to Neo Long 3-5 with tag which elutes at 13.4ml and Neo Long 3-5 without tag which elutes at 13.1ml **(Figure 6).**

Figure 3. Western Dot Blot image of clones secreting Neogenin. **A**. Dot Blot image of clones secreting Neogenin Long 3-5. **B**. Dot Blot image of clones secreting Neogenin Short 3-5. Cells were induced with Doxycyline. Secreted protein with strep tag was visualized through Chemiluminescence with strep tag specific Anti Step-tag II monoclonal antibody conjugated to horseradish peroxidase. Positive control – DCC with strep tag Negative Control -DCC without tag

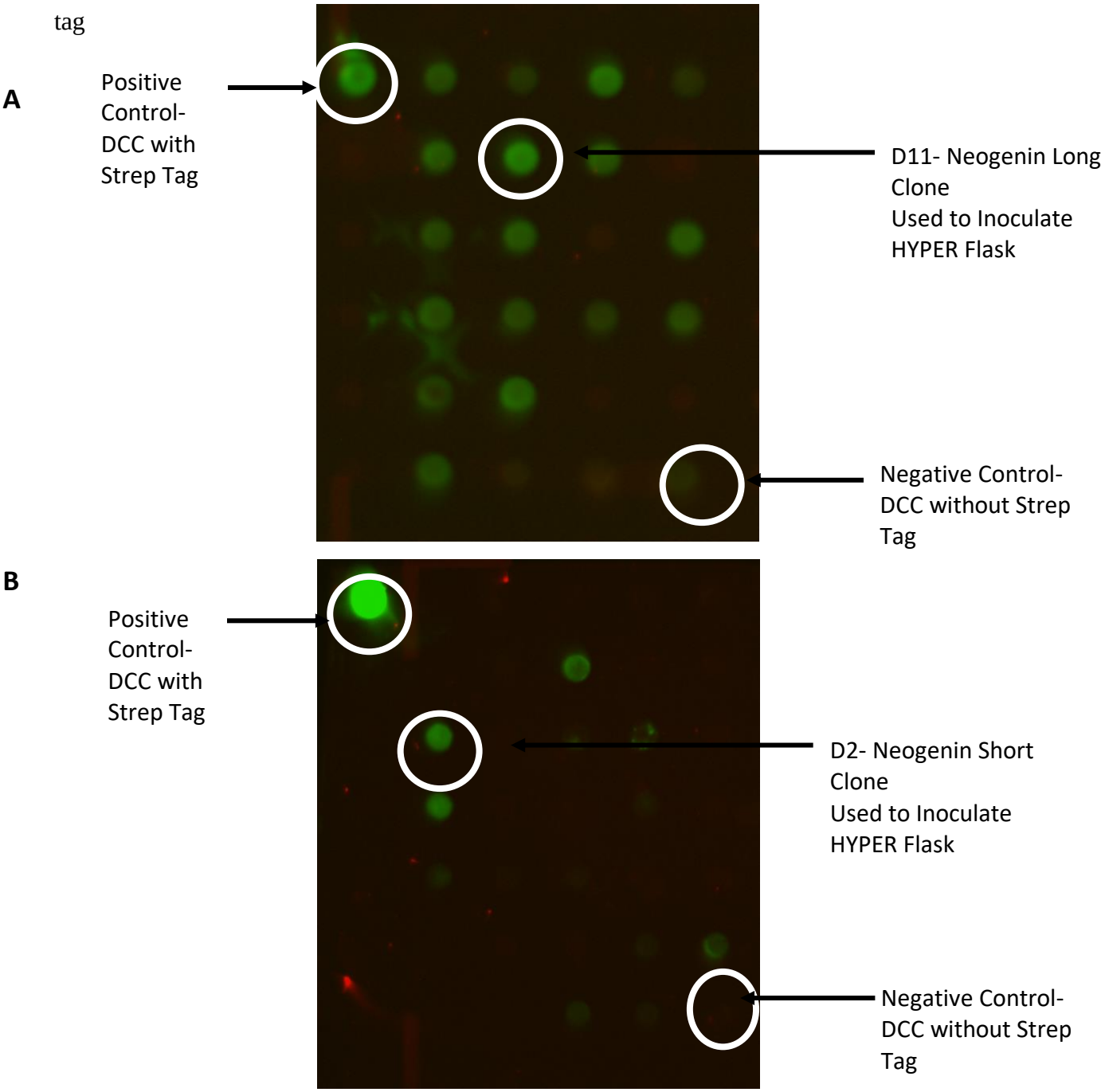

Figure 4. SDS PAGE Gel Images of samples collected of chNet△C, Neo Long 3-5, Neo Short 3-5 and their complexes. All samples were run on 8% SDS- PAGE Gel.

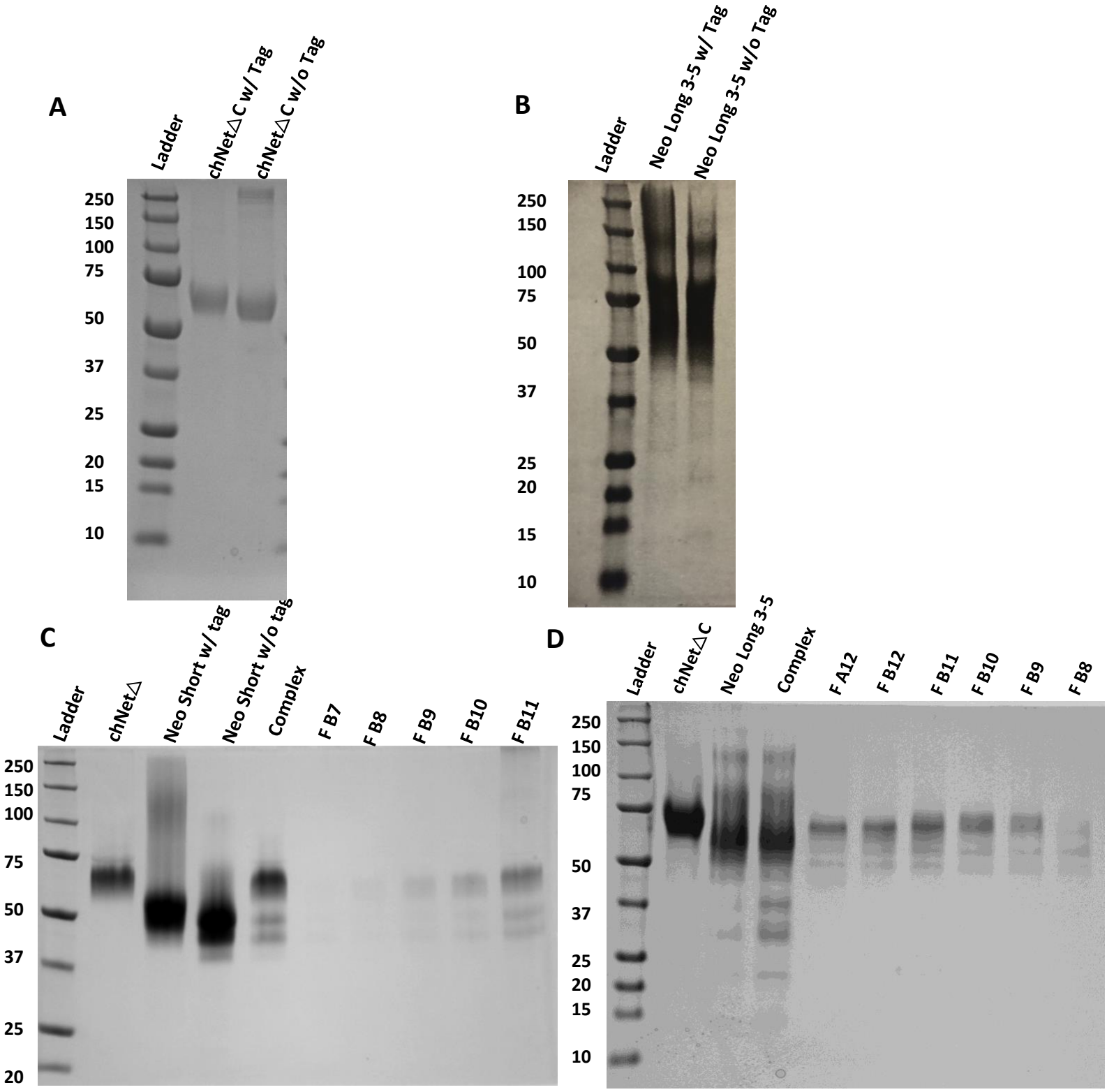

Figure 5. Elution profiles of Neogenin Short 3-5 with Strep tag and Neogenin Short 3-5 without Strep tag acquired from the Superdex 200 10/300 GL size exclusion chromatography column. The following colour scheme was used: Neo Short 3-5 with strep tag, *blue*; Neo Short 3-5 without Strep tag, *green*. All species were eluted in 50mM Tris, pH 7.5 200mM NaCl.

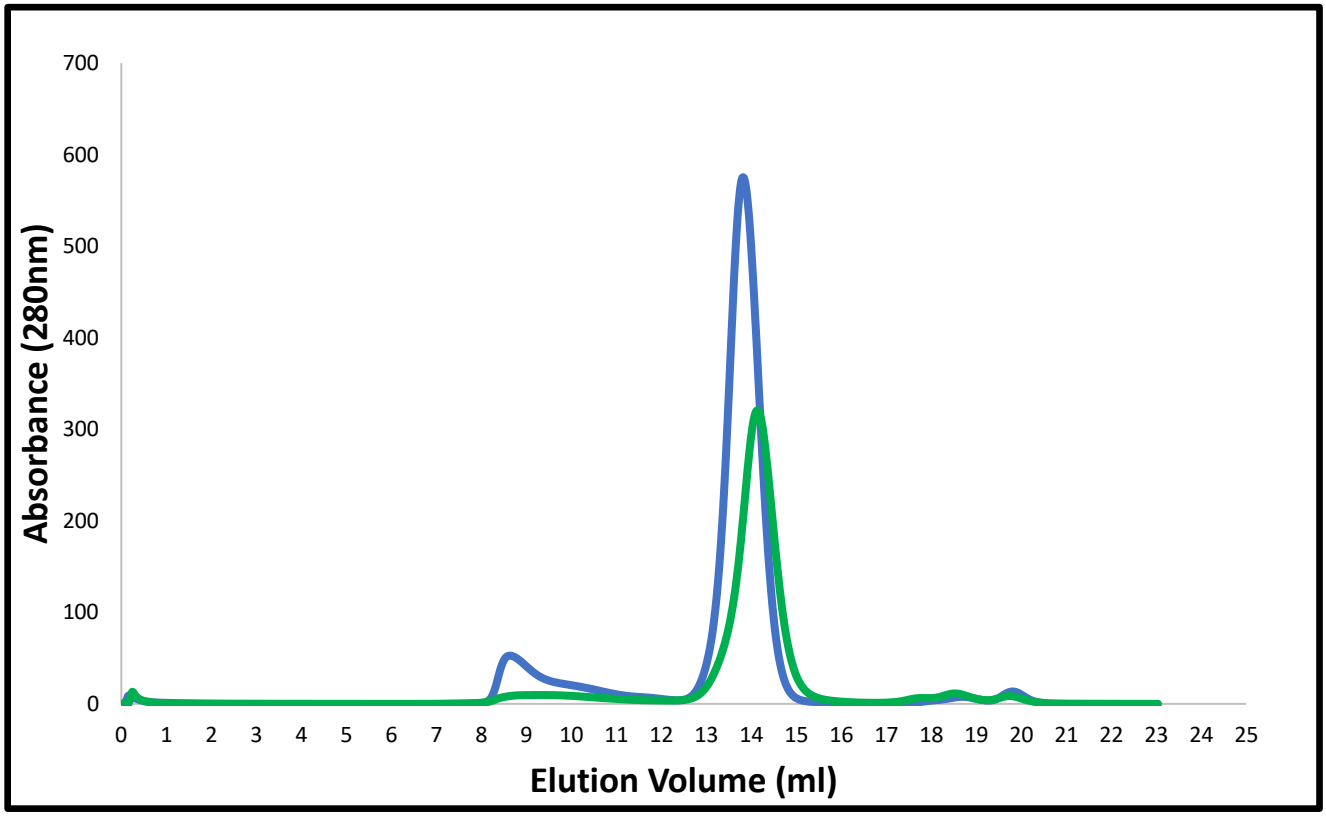

Figure 6. Elution profiles of Neogenin Long 3-5 with Strep tag and Neogenin Long 3-5 without Strep tag acquired from the Superdex 200 10/300 GL size exclusion chromatography column. The following colour scheme was used: Neo Long 3-5 with strep tag, *purple*; Neo Long 3-5 without Strep tag, *red*. All species were eluted in 50mM Tris, pH 7.5 200mM NaCl.

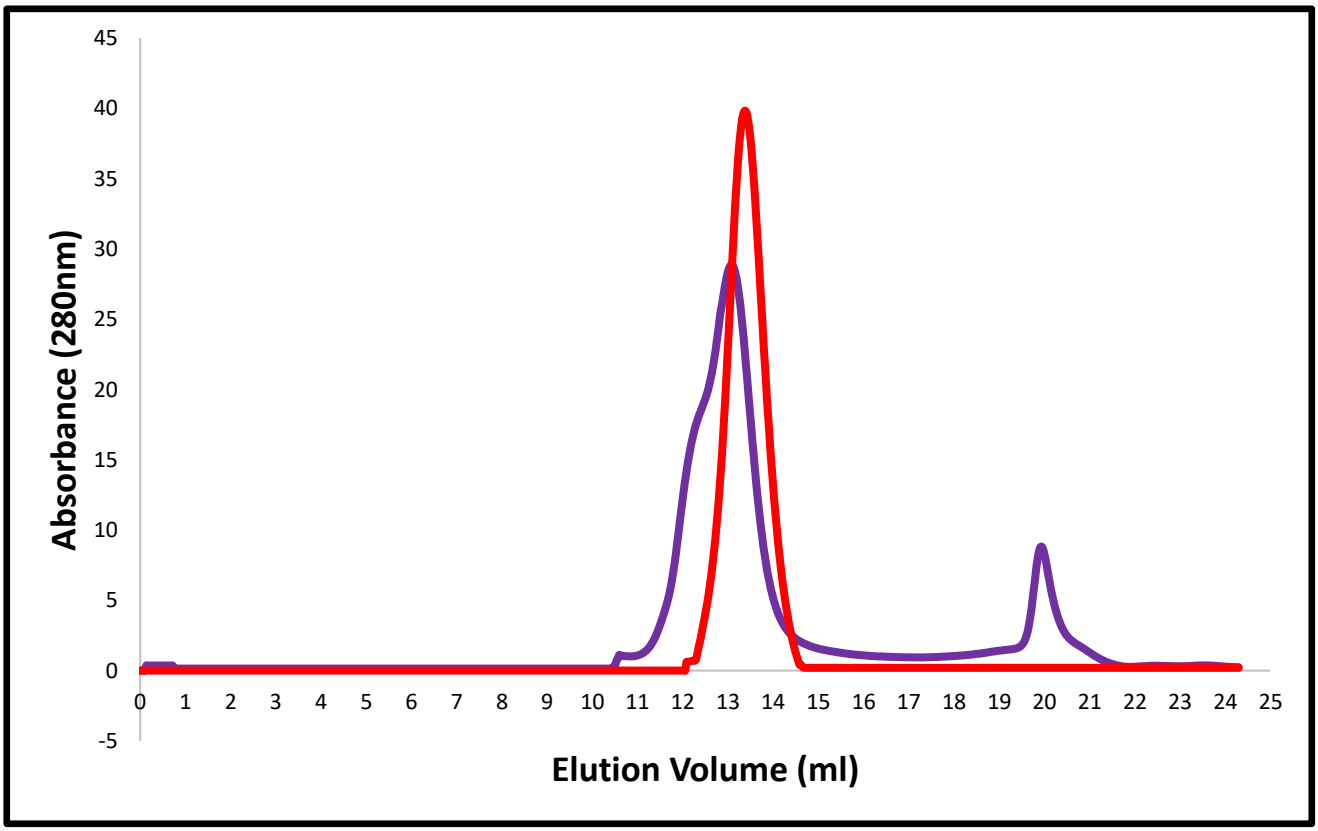

3.2 CHNETΔC- NEO LONG 3-5 AND CHNETΔC- NEO SHORT 3-5 COMPLEX FORMATION

To ensure successful complex formation between the receptor Neogenin and Netrin, the complex was purified on Superdex 200 10/300 GL SEC column and run with 50mM Tris, pH 7.5 200mM NaCl. Elution volume of the receptors Neo short 3-5, Neo Long 3-5 and chNetΔC on the SEC chromatogram were compared with the elution volumes of their complex. Proteins with a bigger molecular weight elute out sooner as compared to proteins of smaller molecular weight. Therefore, a distinction between the elution volumes gives insight into complex formation. The elution volume of Neo Long 3-5 is 13.6ml, that of chNetΔC is 11.8ml and that of the Neo Long 3-5 - chNetΔC complex is 10.6ml **(Figure 7)**. The elution volume of Neo short 3-5 to be 14.2ml, that of chNetΔC is 11.8ml and that of the Neo Short 3-5 - chNetΔC complex is 10.5ml **(Figure 8)**. The significant difference between the elution volumes of the proteins alone as compared to the elution volumes of the complex, suggest successful complex formation.

Figure 7. Elution profiles of Neogenin Long 3-5 without Strep tag, chNetΔC and their complex, acquired from the Superdex 200 10/300 GL size exclusion chromatography column. The following colour scheme was used: Neo Long 3-5 without strep tag, *red*; chNetΔC, *brown*; Neo Long3-5 • chNetΔC, *blue*. All species except chNetΔC were eluted in 50mM Tris, pH 7.5 200mM NaCl. ChNetΔC was eluted in 50mM Tris, pH 7.5 1M NaCl.

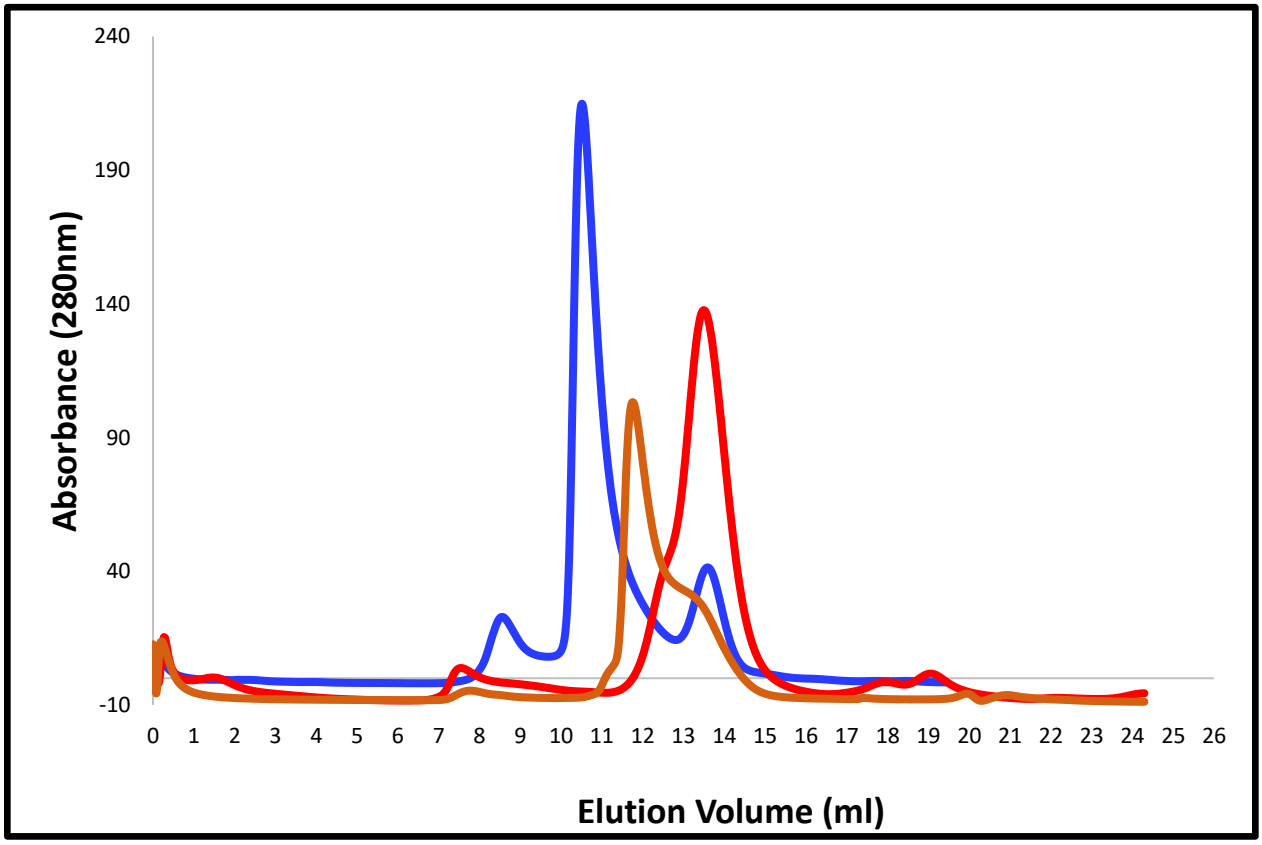

Figure 8. Elution profiles of Neogenin Short 3-5 without Strep tag, chNetΔC and their complex, acquired from the Superdex 200 10/300 GL size exclusion chromatography column. The following colour scheme was used: Neo Short 3-5 without strep tag, *green*; chNetΔC, *brown*; Neo Short 3-5 • chNetΔC, *yellow*. All species except chNetΔC were eluted in 50mM Tris, pH 7.5 200mM NaCl. ChNetΔC was eluted in 50mM Tris, pH 7.5 1M NaCl.

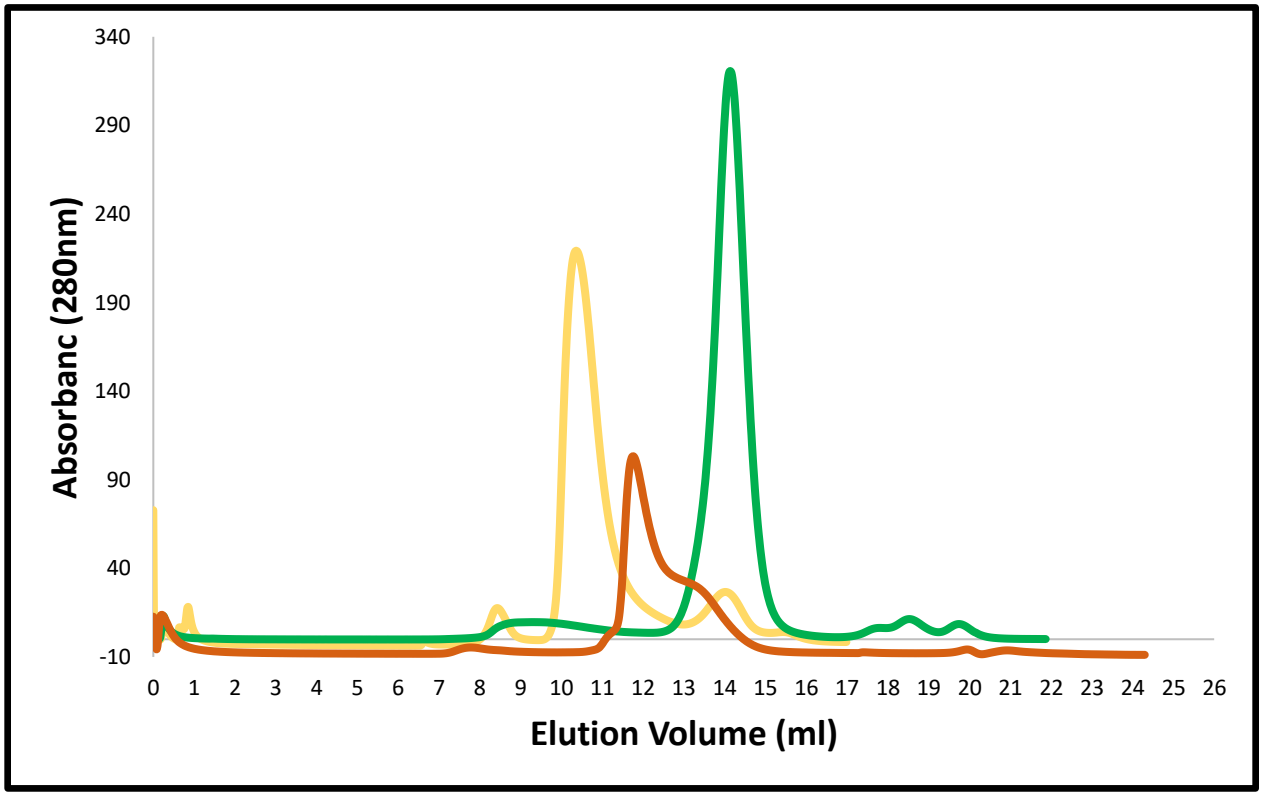

3.3 CHNETΔC, NEO LONG 3-5, NEO SHORT 3-5, CHNETΔC- NEO LONG 3-5 AND CHNETΔC- NEO SHORT 3-5 COMPLEX IN SOLUTION

DLS measurements of Neo Long 3-5 alone and in complex with chNet△C were conducted prior to SAXS data collection and reveal the presence of monodisperse species in solution **(Figure 9).** The R_H values of Neo Long 3-5 alone is 4.4± 0.3nm and that of the complex is 7.2± 0.1nm. This difference in the R_H values can be attributed to a larger molecule as a consequence of complex formation (37).

SAXS data for chNetΔc, Neo Long 3-5, Neo Short 3-5, chNetΔc- Neo Long 3-5 and chNetΔc- Neo Short 3-5 complex was collected at ~9mg/ml concentration to obtain low resolution information on the protein behaviour. Scattering curves were buffer subtracted and merged to generate SAXS plots.

The P*(r)* distribution function gives the paired set of distances between all the electrons in the macromolecular structure (38,39). The P*(r)* distribution of Neo Long 3-5 and Neo Short 3-5, both depict a single peak with a longer tail, characteristic of an elongated macromolecule **(Figure 10A and B)**. The P*(r)* distribution of chNet△C depicts a single prominent peak and a smaller less prominent peak, signifying a protein of multiple domains **(Figure 10A and B).** The complexes, chNet△C- Neo Long 3-5 and chNet△C- Neo Short 3-5 both show *P(r)* distributions with a single broad peak, signifying proteins of a globular shape **(Figure 10A and B).**

The Kratky analysis of the biological macromolecules give information on the unfolded-ness and overall shape of the macromolecule (38). Kratky plots of chNet△C, along with Neo Long and Neo Short, demonstrate a bell-shaped curve representative of a globular macromolecule. However, these molecules also represent partial unfoldedness due to the slight plateau as the curve descends, indicating their "extended" like shape **(Figure 11A and 11C).**

Analysis of the chNet△C – Neo Long complex and chNet△C- Neo Short complex depict a sharper bell curve and therefore confirm a macromolecule of globular shape **(Figure 11A and 11C).**

The merged SAXS data for the chNet△C and Neo Long 3-5 proteins alone were processed using the *P(r)* analysis to obtain the R_g and D_{max} values. The R_g and D_{max} values of chNet△C were 57.45 ±0.3 and 198.1nm respectively, and that of Neo Long 3-5 were 41.30 (±0.1) and 162.3nm respectively **(Table 1).** The *P(r)* function calculated from the SAXS data of the complex differs from that of chNet△C and Neo Long 3-5 proteins alone. The merged SAXS data for the complex were processed using the *P(r)* analysis to obtain a R_g value of 60.12 (±0.1) and a D_{max} value of 240.9nm **(Table 1).**

Similarly, the *P(r)* function calculated from the SAXS data of the chNetdC- Neo Short 3-5 complex differs from that of chNet△C and Neo Short 3-5 proteins alone. The R_g and D_{max} values of chNet△C were 57.45 ±0.3 and 198.1nm respectively, and that of Neo Short 3-5 were 41.00 (±0.1) and 157.8nm respectively **(Table 2).** The R_g and D_{max} values of the complex were 67.21 (±0.1) and 252.0nm, respectively **(Table 2).**

Table 1. Summary of the Hydrodynamic Parameters for chNetΔC, Neo Long 3-5 and chNetΔC-Neo Long 3-5 complex.

Parameters	chNetΔC	Neo Long 3-5	chNetΔC-Neo Long 3-5 Complex
R_H (A°)[a]	-	44.01 (±0.3)	72.07 (±0.1)
Rg(A°)[b]	57.43 (±0.3)	41.30 (±0.1)	60.12 (±0.1)
Dmax (A°)[b]	198.1	162.3	240.9
Rg (A°)[c]	57.00 (±0.3)	41.87(±0.2)	60.16(±0.3)
Dmax (A°)[c]	195.4	156.2	248.6
R_H (A°)[d]	-	41.24	72.07
Chi[e]	1.30	1.20	1.34
Rg (A°)[f]	48.93	41.58	57.76
Dmax (A°)[f]	180.49	147.29	206.1
Chi[g]	6.79e-01	3.32e-01	1.98

Table 2. Summary of the Hydrodynamic Parameters for chNetΔC, Neo Short 3-5, and chNetΔC-Neo Short 3-5 complex.

Parameters	chNetΔC	Neo Short 3-5	chNetΔC-Neo Short 3-5 Complex
Rg (A°)[b]	57.43 (±0.3)	41.00 (±0.1)	67.21 (±0.1)
Dmax (A°)[b]	198.1	157.8	252.0
Rg (A°)[c]	57.00 (±0.3)	40.76(±0.2)	67.24(±0.3)
Dmax (A°)[c]	195.4	155.8	254.1
Chi[e]	1.30	1.32	1.35
Rg (A°)[f]	48.93	40.27	64.52
Dmax (A°)[f]	180.49	141.73	220.58
Chi[g]	6.79e-01	1.73e-01	1.38

[a]The values were experimentally determined from DLS with error obtained from linear regression analysis to infinite dilution for multiple concentrations.
[b] Experimentally determined using GNOM analysis from SAXS Data
[c]Parameters obtained from DAM Models
[d]Model-based parameters calculated from HYDROPRO
[e] Goodness of fit parameter suggesting agreement between raw data and data back calculated from *ab intio* model DAMMIN
[f]Experimentally determined using DENSS
[g]Goodness of fit parameter suggesting agreement between raw data and data back calculated from *ab intio* model DENSS

Figure 9. Dynamic light scattering profiles of Neo Long 3-5 alone and its complex with chNet△C. The concentration dependence of the R_H of Neo Long 3-5 and its complex is shown in figure B and C. All samples were analyzed in 50mM Tris, pH 7.5, 200mM NaCl.

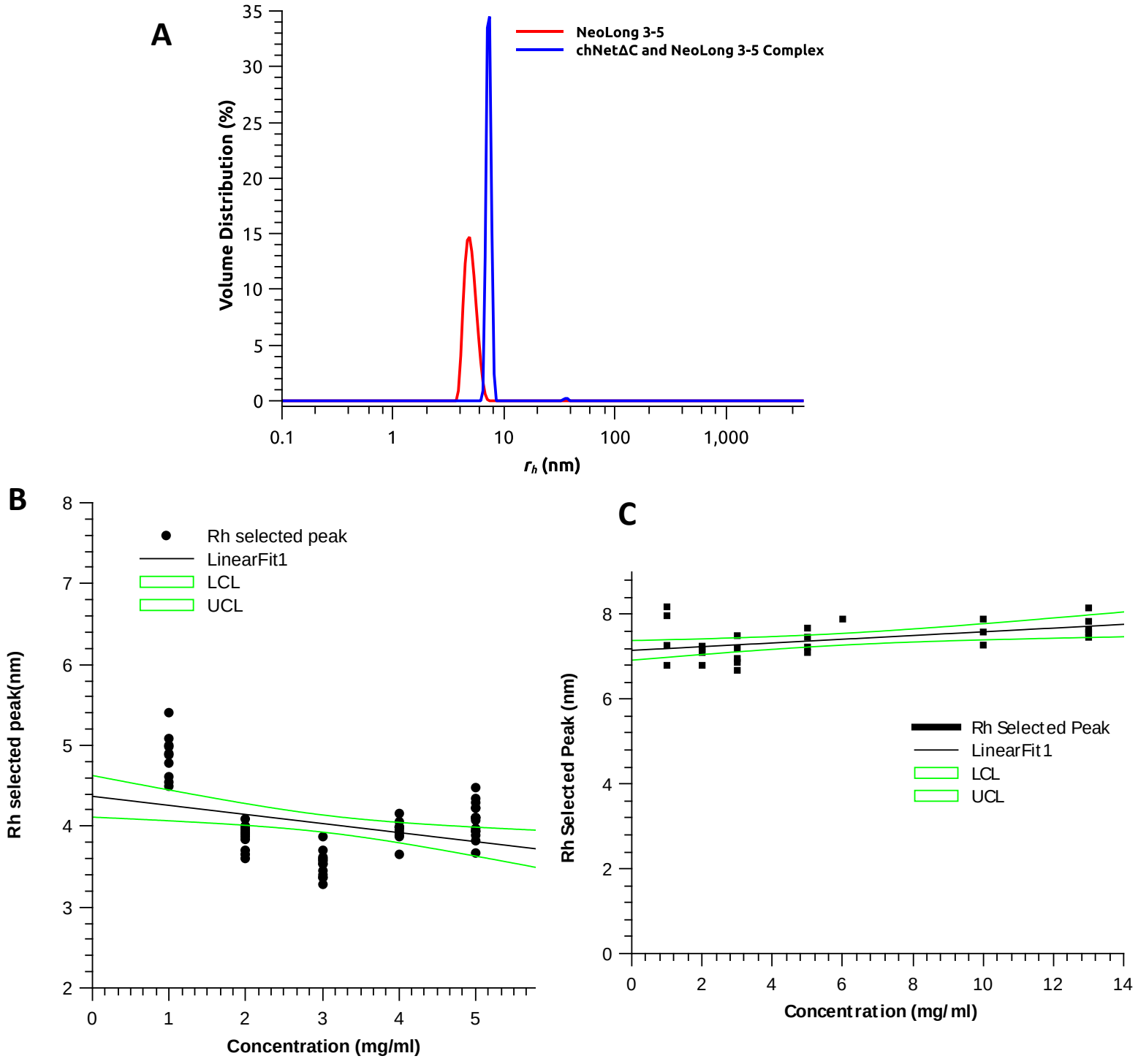

Figure 10. Normalised Pair distribution function of chNet△C and Neogenin alone and in complex obtained from SAXS Data. The data was collected in 50mM Tris, pH 7.5, 200mM NaCl.

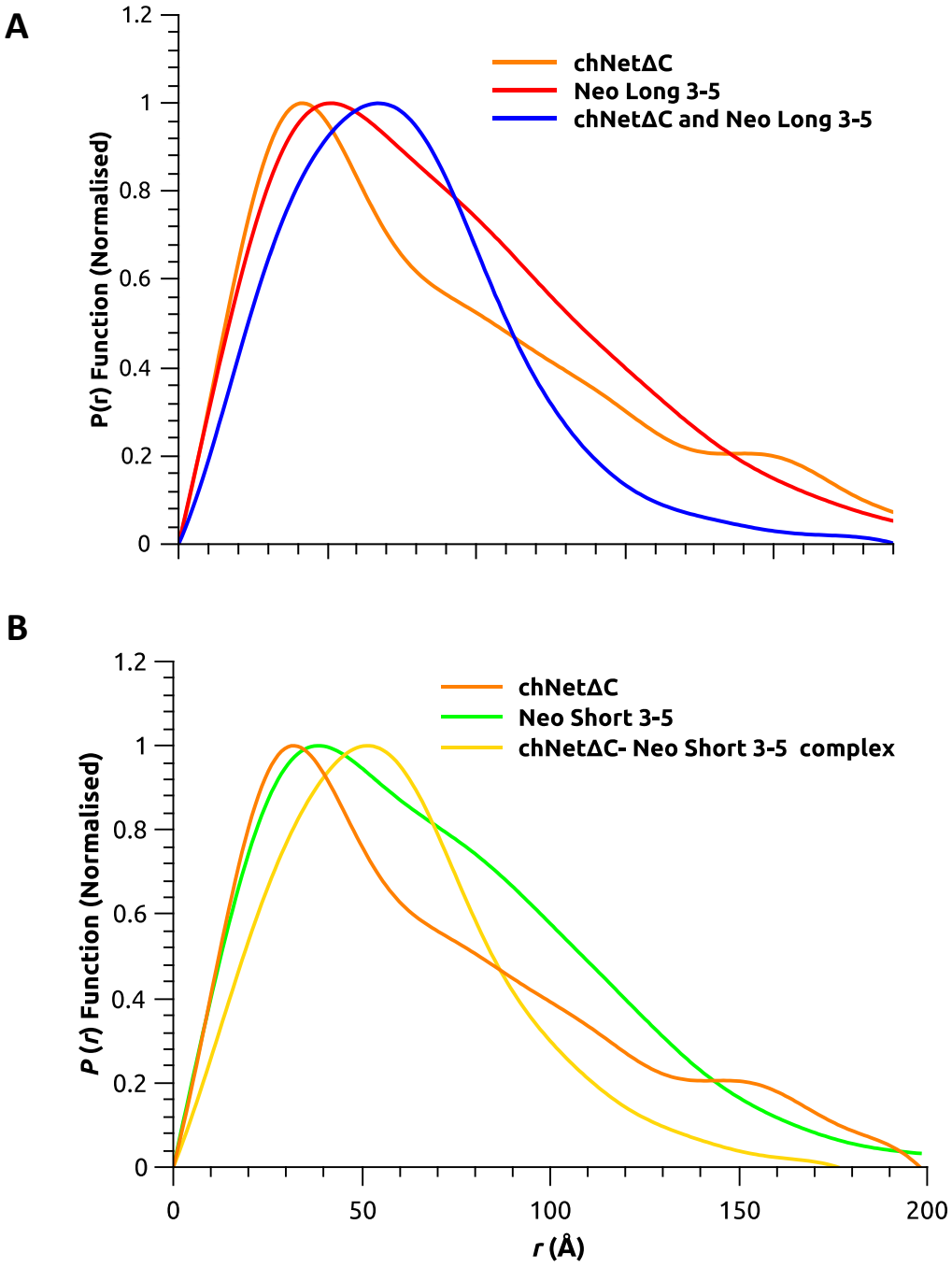

Figure 11. Kratky plots for chNetΔC, Neogenin alone and in complex obtained from SAXS data. The data was collected in 50mM Tris, pH 7.5, 200mM NaCl.

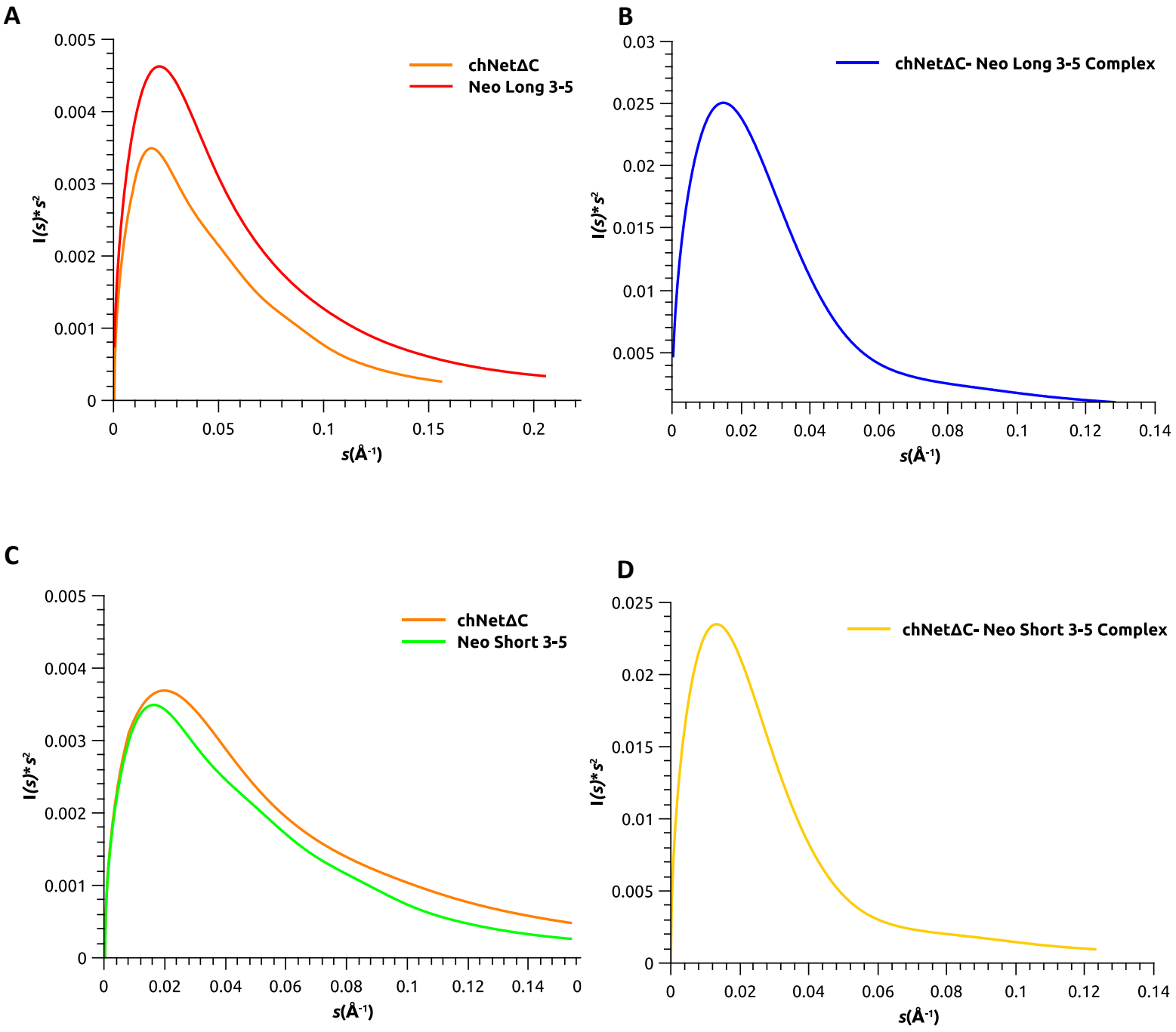

The DENSS algorithm reconstructs 3D electron densities from 1D solution scattering data. The algorithm uses a mathematical approach called "Iterative phase retrieval" to construct density models (40). The program calculates the density and provides a R_g value which is the radius of gyration calculated from the density map and as well a Chi_2 value which provides the goodness of fit between the calculated density and the interpolated experimental data (40). Density models were constructed for chNet△C, Neo Long3-5, Neo Short 3-5 and their complexes **(Figure 13 and 14).** The experimental R_g, D_{max} and χ^2 value of chNet△C, Neo Long 3-5 and Neo Short 3-5 are as follows: 48.93A°, 180.49A° and 6.79e-01, 41.58A°, 147.29A° and 3.32e-01, and 40.27A°, 141.73A° and 1.73e-01, respectively **(Table 1 and 2)**. The R_g values of the proteins alone differ from that of the complex. The R_g, D_{max} and χ^2 value of chNet△C- Neo Long3-5 complex is 57.76A°, 206.1A° and 1.98, respectively **(Table 1).** Similarly, the R_g , D_{max} and χ^2 value of chNet△C- Neo Short 3-5 complex is 64.52 A°, 220.58 A°, and 1.38, respectively **(Table 2).** Scattering profiles provided fit well and show convergence with the interpolated data from DENSS **(Figure 12).**

Low-resolution shape reconstruction using the DAMMIN program, suggests an extended shape conformation of chNet△C, Neo Long3-5 and Neo Short 3-5 **(Figure 16, 17A, 18A).** DAMMIN structures of the chNet△C-Neo Long3-5 complex and chNet△C- Neo Short 3-5 complex demonstrate a larger structure with at least 2 molecules present **(Figure 17B and 18B)** (41). The χ^2 value of 1.30, 1.20, 1.34, 1.32 and 1.35 for chNet△C, Neo Long 3-5, chNet△C-Neo Long 3-5 complex, Neo Short 3-5, chNet△C- Neo Short 3-5 indicate that the individual models agree well with the SAXS data **(Table 1 and 2).** Scattering data superimposed with

scattering profiles calculated from the low resolution DAMMIN models show high convergence between the data sets **(Figure 15).**

In order to confirm the parameters obtained from DLS for Neo Long 3-5 and its complex with chNet△C, agree with that of the DAM models, HYDROPRO was used. The R_H values obtained from HYDROPRO for the DAM models of Neo Long 3-5 and chNet△C-Neo Long 3-5 were 41.24A° and 72.07 A°, respectively **(Table 1).** In comparison to the R_H values obtained for Neo Long 3-5 and chNet△C-Neo Long 3-5 through DLS (44.01 (±0.3) A° and 72.07(±0.1) A°) **(Table 1),** these values are in close proximation to those obtained by DLS and hence, we can safely conclude the parameters obtained are not an artifact.

Figure 12. Measured Data for chNet△C, Neogenin and their complexes is superimposed with the scattering profiles calculated based on the 3D electron density models constructed through DENSS shown in Figure 14 and 15. A. chNet△C B. Neo Long 3-5 C. Neo Short 3-5 D. chNet△C - Neo Long 3-5 complex E. chNet△C - Neo Short 3-5 complex

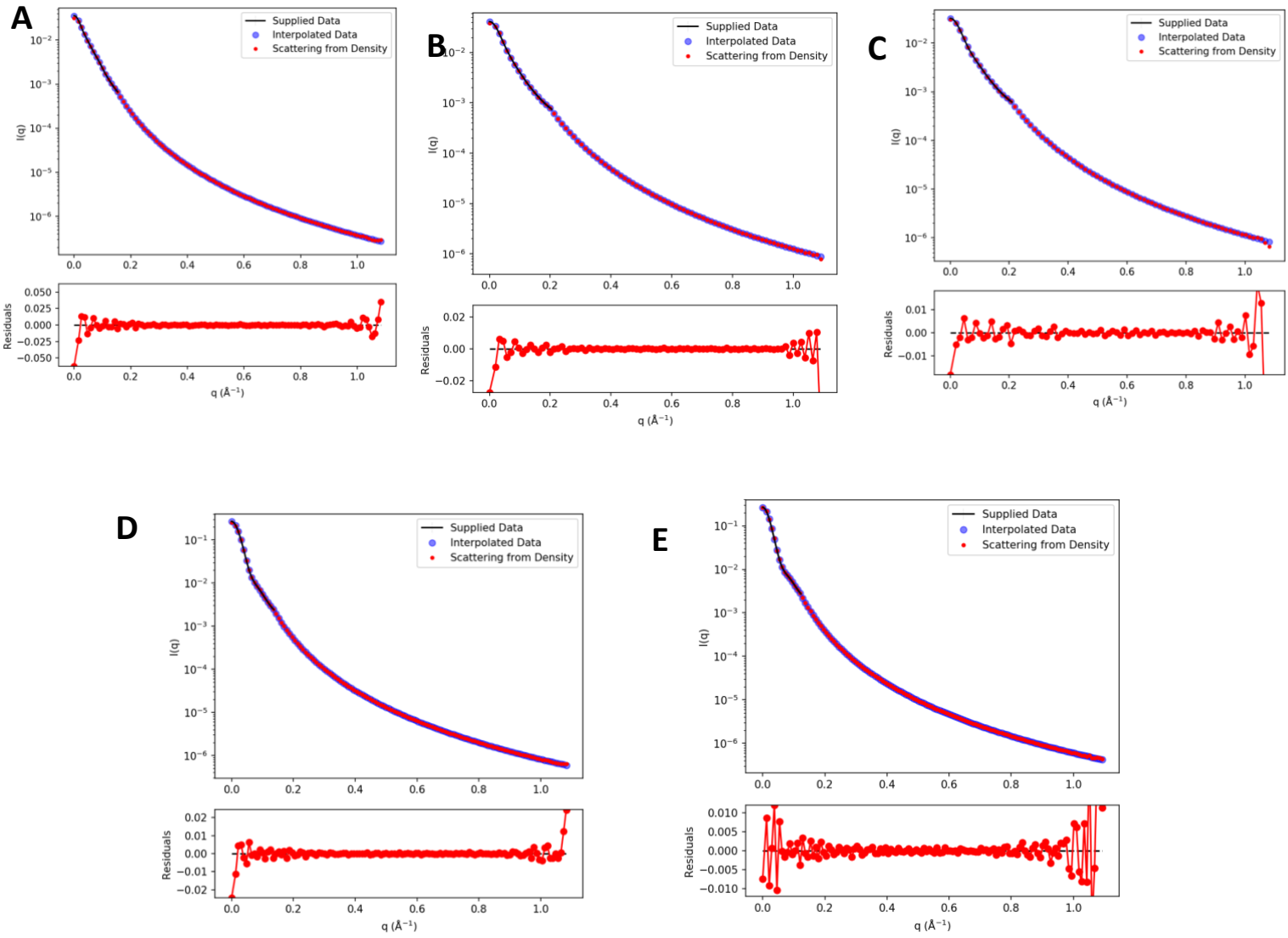

Figure 13. Electron density reconstructions from experimental solution scattering data. 3D electron densities of (A) chNetΔC, (B) chNet△C superimposed with high resolution chNet△C structure (PDB: 4OVE) (C) Neo Long 3-5 (D) Neo Short 3-5. Models were constructed using the DENSS algorithm.

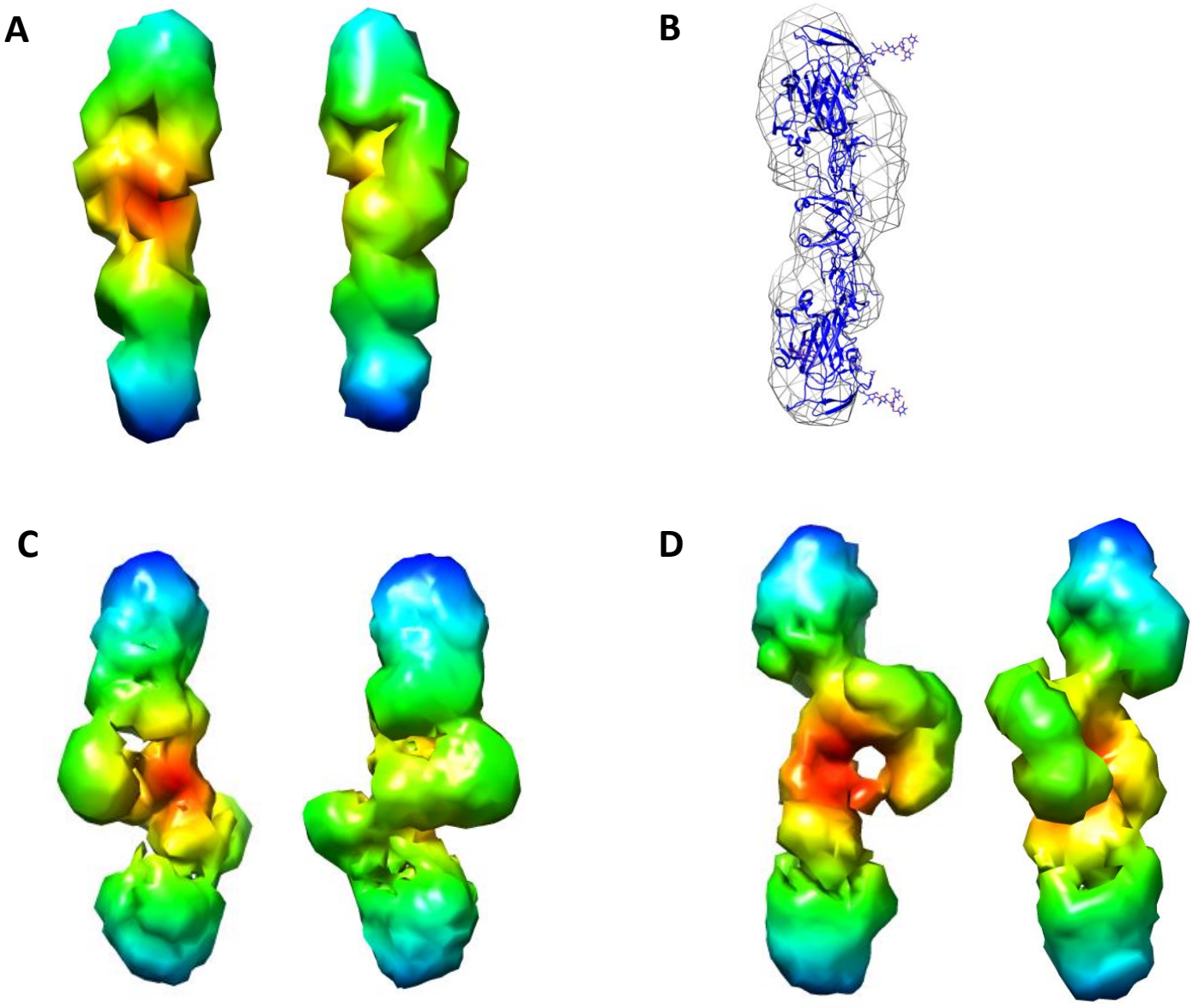

Figure 14. Electron density reconstructions from experimental solution scattering data. 3D electron densities of (A) chNetΔC- Neo Long 3-5 complex (B) chNet△C- Neo Short 3-5 complex. Models were constructed using the DENSS algorithm.

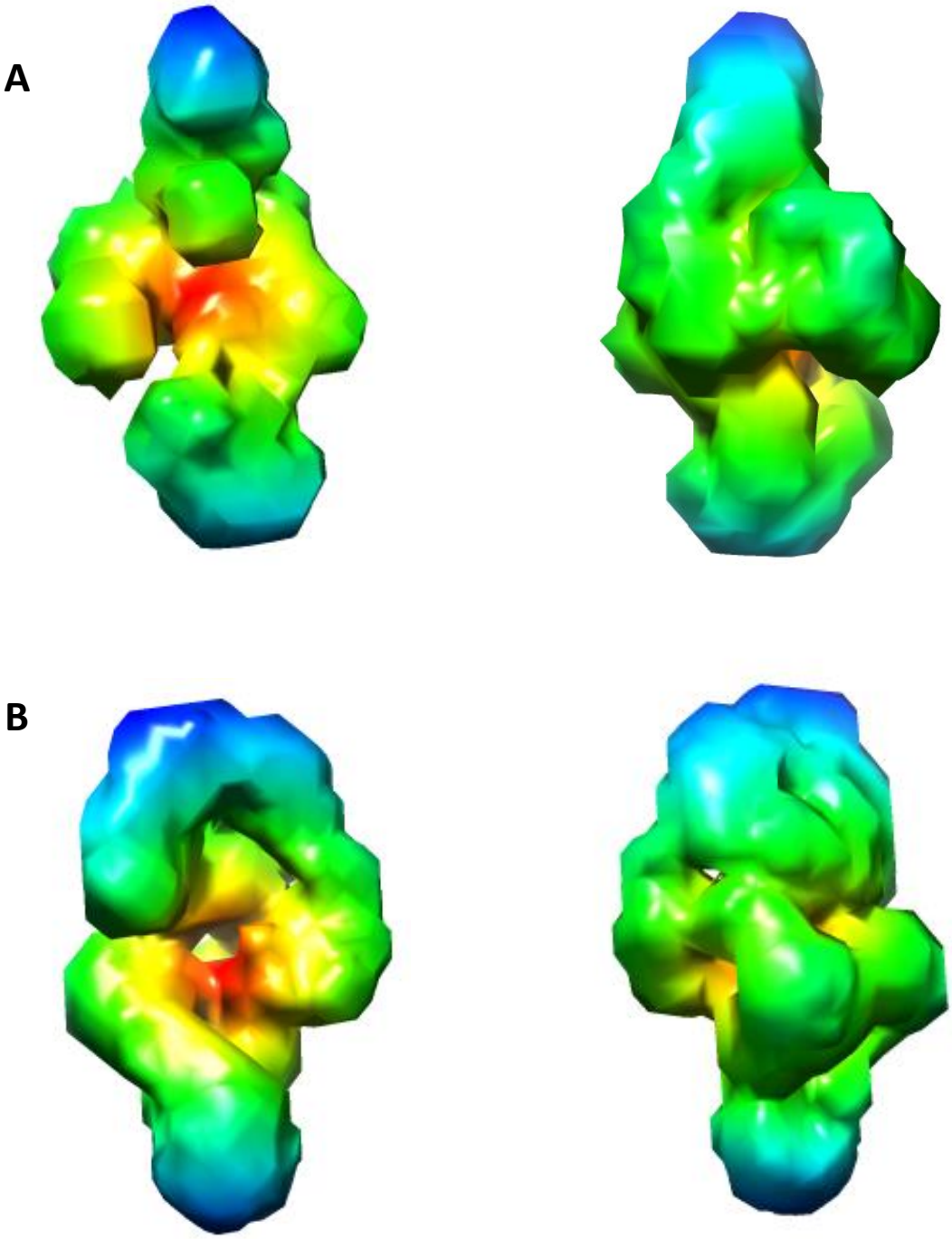

Figure 15. Solution conformation of chNetΔC, Neogenin and their complexes determined by SAXS. The merged measured data for Neogenin and its complexes is superimposed with the scattering profiles calculated based on the low resolution DAMMIN models in figures 16,17 and 18.

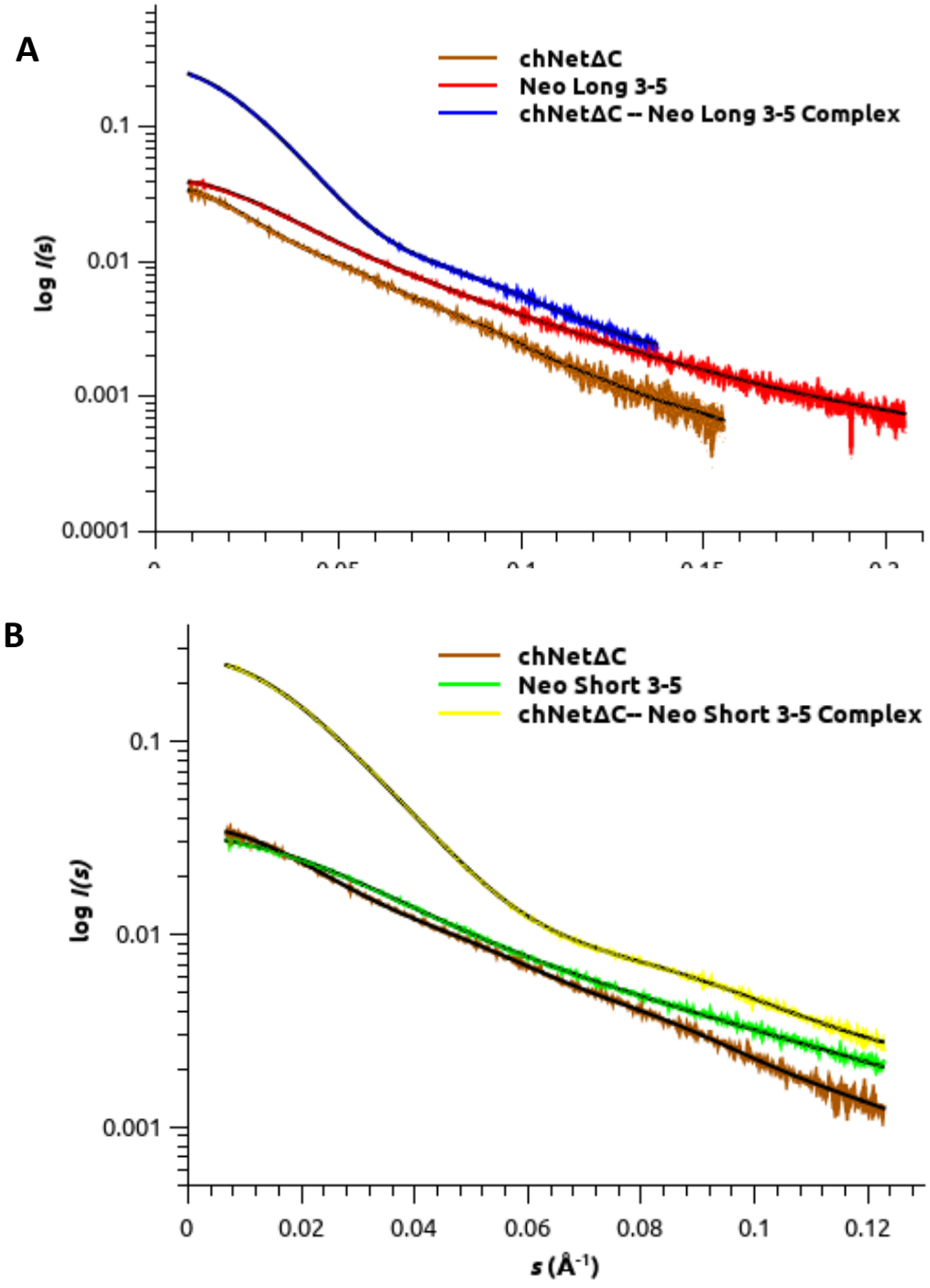

Figure 16. Low resolution model of chNetΔC. Model was determined by DAMMIN.

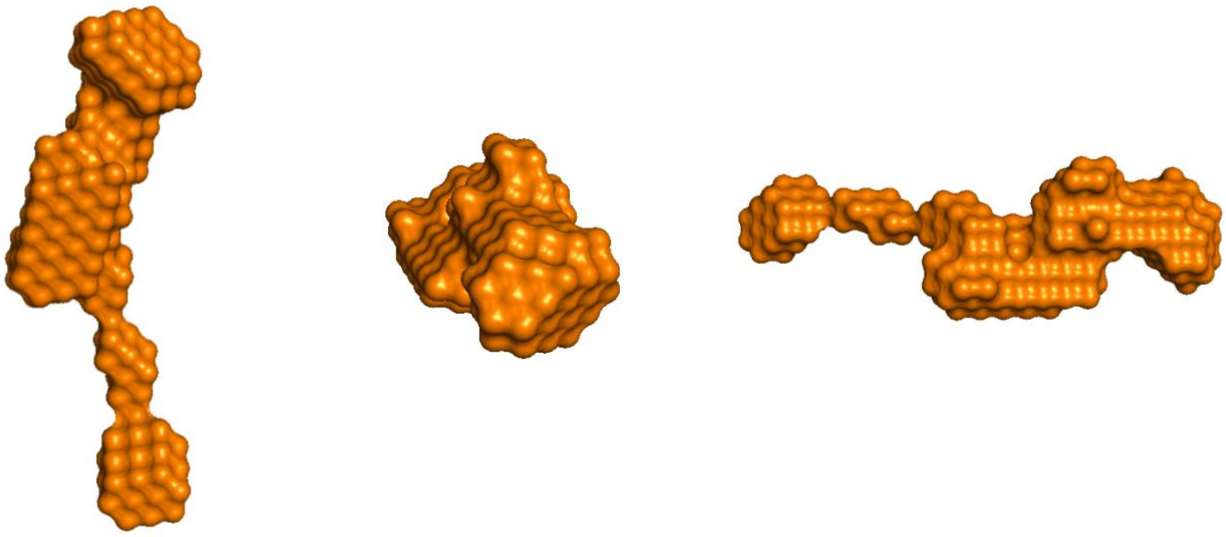

Figure 17. Low resolution models of Neo Long 3-5 and chNetΔC -Neo Long 3-5 complex.

Low resolution model of (A) Neo Long 3-5 (red) and (B) chNetΔC -Neo Long3-5 complex (blue) determined by DAMMIN.

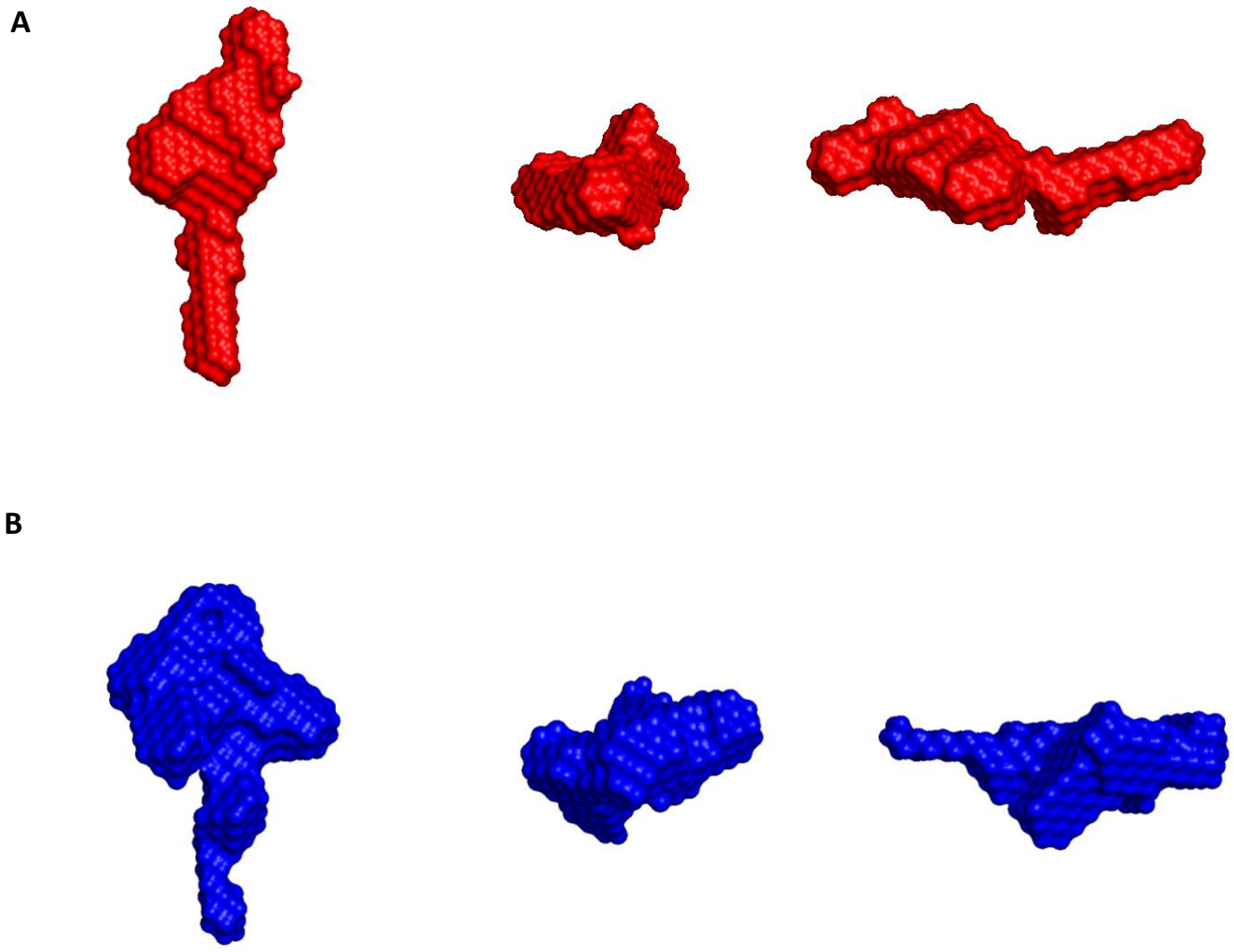

Figure 18. Low resolution models of Neo Short 3-5 and chNetΔC -Neo Short 3-5 complex.

Low resolution model of (A) Neo Short 3-5 (red) and (B) chNetΔC -Neo Short 3-5 complex (blue) determined by DAMMIN.

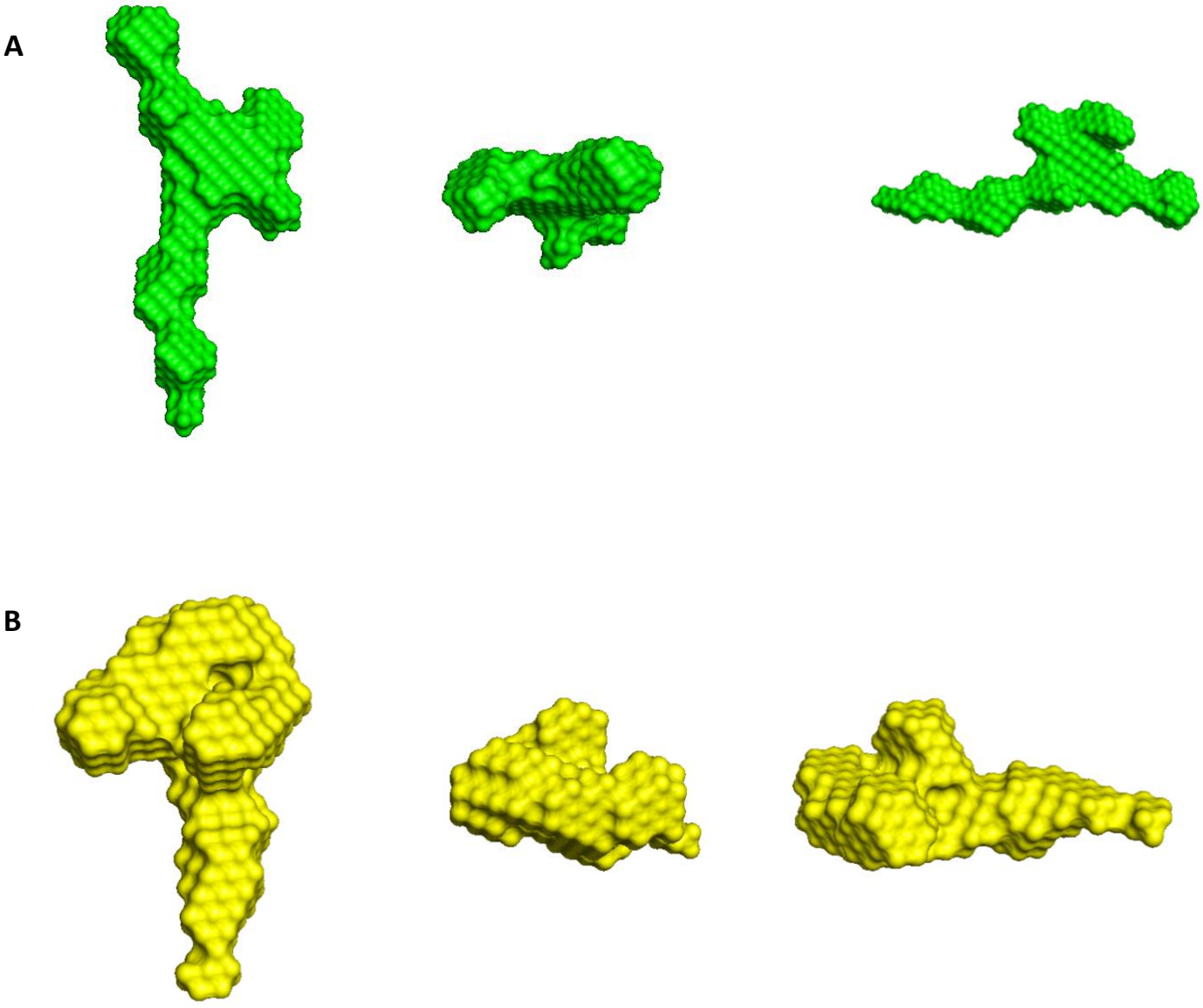

3.4 CRYSTALLIZATION TRIALS

Several commercial crystallization screen from Jenna Biosciences and Hampton Research were used to test crystallization solutions for a condition suitable for crystallization of chNet△C-Neo Long 3-5 complex and chNet△C-Neo Short 3-5 complex. The complex chNet△C-Neo Long 3-5 was tested at a concentration of 12.5mg/ml and chNet△C-Neo Short 3-5 complex was tested at 9.3mg/ml. Both complexes only crystallized in wells containing solution form JBScreen Classics 7. The solution condition for chNet△C-Neo Long 3-5 complex crystals was: 47% w/v 2-methyl-2,4- pentanediol 100mM HEPES, pH 7.5. Similarly, the solution condition for chNet△C-Neo Short 3-5 complex crystals was: 35% w/v 2-methyl-2,4- pentanediol 100mM Imidazole, pH 8.0 (42). All crystals varied in shape and size, with some more round and some with a more elongated shape.

Figure 19. Image of crystals of chNet△C- Neo Long 3-5 Complex grown in sitting well drop in 47% w/v 2-methyl-2,4- pentanediol 100mM HEPES, pH 7.5. Sitting drops were prepared by adding 1μL of reservoir solution to 1μL of chNet△C- Neo Long 3-5 Complex at 12.4mg/ml.

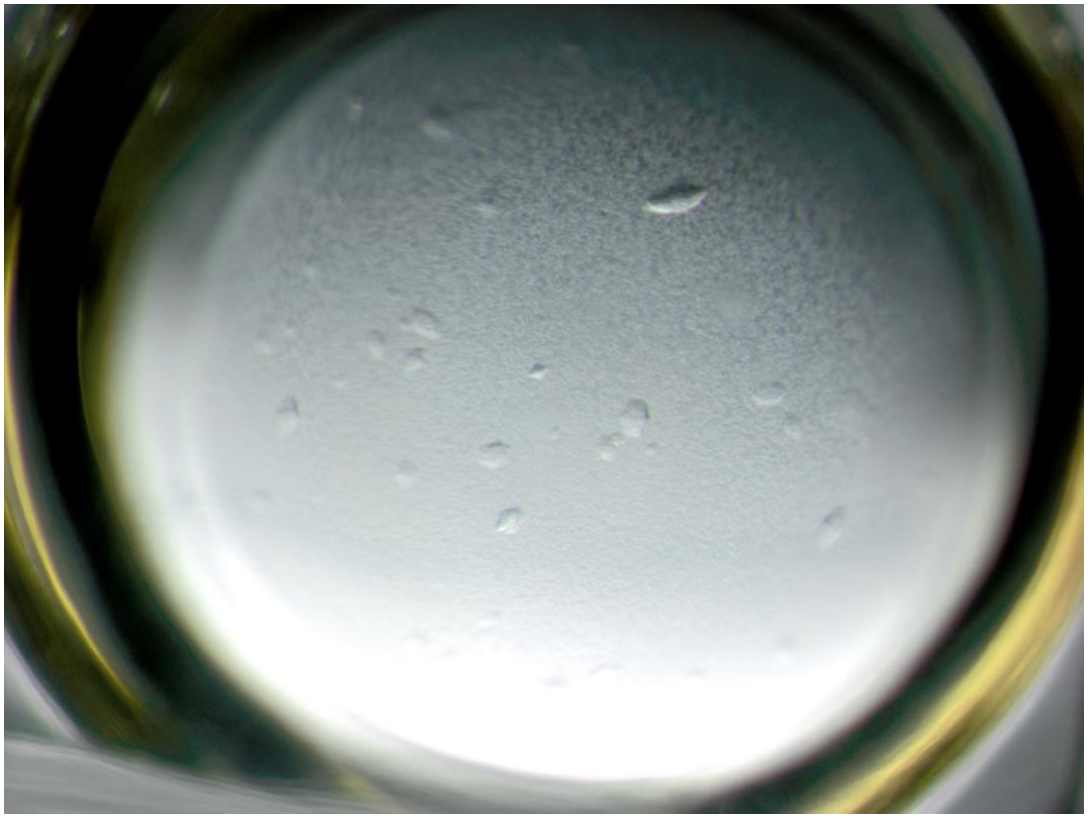

Figure 20. Image of crystals of chNet△C- Neo Short 3-5 Complex grown in sitting well drop in 35% w/v 2-methyl-2,4- pentanediol 100mM Imidazole, pH 8.0. Sitting drops were prepared by adding 1μL of reservoir solution to 1μL of chNet△C- Neo Short 3-5 Complex at 9.3mg/ml.

4. Discussion

Netrin has been identified as a laminin related protein which plays a key role in axon guidance. As Netrin binds to its receptor Neogenin, it promotes chemoattraction and hence morphogenesis, which can promote cancer cell migration and proliferation. While the interaction of Netrin with its receptor DCC Is well understood, much more research needs to be conducted on Neogenin. For this reason, we have employed the use of biophysical approaches to better understand the binding of Netrin to Neogenin. Previous structural studies using X-Ray Crystallography have been conducted on truncated versions of Neogenin and their interaction with Netrin. This research concluded that Netrin and Neogenin interact with one another in a 2:2 Heterotetramer, implying that in order for successful interaction between the ligand and receptor, two molecules of both must be present. Furthermore, they propose the interaction includes, the FN4 region of Neogenin interacts with the LN region on the N terminus of Netrin and the FN5 region of Neogenin interacts with the LE3 region on the C terminus of Netrin. As such the interaction of two molecules of Netrin with two molecules of Neogenin, forms an X shaped heterotetramer. The goal in our research was to further the current studies on the interaction by using constructs of Neogenin which include FN regions 3-5. Elucidating the binding interaction of Netrin to its receptor Neogenin will allow us insight into their mechanism of action and potential to design a drug candidate to halt such an interaction.

Our biophysical studies revealed that our chNet△C is dimeric in solution. A previously resolved crystal structure **(Figure 1, PDB 4OVE)**, reveal chNet△C to have an elongated structure. Our 3D electron density models from DENSS and model from DAMMIN, demonstrate

similar results and depict chNet△C as a molecule of elongated shape. Furthermore, overlapping the electron density map with the crystal structure **(Figure 13B)** reveals chNet△C to be a dimer.

According to the different constructs used in our research, Neo Long 3-5 with a linker region should be longer than the Neo Short 3-5 construct which lacks the linker region. This difference between the two constructs can be observed in biophysical data. SAXS data reveal the R_g value and D_{max} value of Neo long 3-5 to be 41.30 (±0.1) nm and 162.3nm, respectively **(Table 1).** As compared to Neo Short 3-5 which has a R_g value of 41.00 (±0.1) nm and a D_{max} value of 157.8nm **(Table 2),** which are both slightly smaller values than that of Neo Long 3-5.

Successful complex formation between chNet△C and Neo Long 3-5 was confirmed through SAXS and DLS. According to DLS analysis the R_H values of Neo Long 3-5 alone is 4.4± 0.3nm and that of the complex is 7.2± 0.1nm. According to data from SAXS, the R_g value of the complex is 60.12 (±0.1) and the D_{max} value is 240.9nm **(Table 1).** This difference in values between the proteins alone as compared to the complex, indicates successful complex formation. Electron density maps obtained from DENSS along with low resolution models from DAMMIN both depict structures that are larger than that of the ligand or receptor alone (**Figure 13, 14, 16-18)**.

Likewise, complex formation between chNet△C and Neo Short 3-5 was confirmed through SAXS. Here the R_g value of the complex is 67.21 (±0.1) and the D_{max} value is 252.0nm **(Table 2).** These values differ from that of the proteins alone and comparatively indicate successful complex formation. Electron density maps obtained from DENSS along with low resolution models from DAMMIN both depict structures that are larger than that of the ligand or receptor alone (**Figure 13, 14, 16-18)**. Previous studies conducted, reveal a 2:2 Heterotetramer conformation upon interaction of chNet△C and Neo Short 4-5. However, no firm conclusions

can be made supporting or rejecting this conclusion through my biophysical assays. An attempt to align a previous crystal structure of Netrin complexed with Neogenin (PDB: 4PLN) to our density map obtained from DENSS rendered unsuccessful. This failure to perfectly align can be attributed to the use of a different Neogenin construct used in their complex formation, which lacks one of the FN regions included in ours. This difference in structures can also suggest that perhaps more than two molecules of each partner are playing a role while interacting. However, due to the nature of these biophysical experiments conducted within solution, models of high enough resolution are not obtained and hence render us from making any solid conclusions on the conformation of the complex.

Through our biophysical approach to elucidate the interaction between chNet△C and different constructs of Neogenin, we can shed some light on complex formation. Although, SAXS and DLS can assure successful complex formation through its experimental parameters, a X-ray crystal structure would be ideal to make any further conclusion on the interaction of the two molecules.

5. Summary and Future Directions

Netrins are axon guidance cue molecules from the laminin related protein family. They play a key role in neuronal navigation, immune cell migration, angiogenesis and cell survival. Netrin is known to have to many binding receptors including DCC, UNC5 and Neogenin.

In this research we used a biophysical approach to study two different constructs of Neogenin; Neo Long 3-5 and Neo Short 3-5. We studied their interaction with chNet△C, to better understand their binding and further their mechanism of action to ideally construct a drug target, halting their interaction. Gel electrophoresis, Size Exclusion Chromatography, dynamic light scattering, and small angle X ray scattering were used to conduct a comprehensive analysis of chNet△C, Neo Long 3-5, Neo Short 3-5 and their complexes. The low resolution SAXS models for the complexes appear larger and more compact than the extended models for the ligand or receptor alone (D_{max} = for 198.1nm chNet△C, D_{max} = 162.3nm for Neo Long 3-5, D_{max} = 157.8nm for Neo Short 3-5 D_{max} = 240.9nm for chNet△C- Neo Long 3-5 complex and D_{max} = 252.0nm for chNet△C- Neo Short 3-5 complex). Two conditions 47% w/v 2-methyl-2,4-pentanediol 100mM HEPES, pH 7.5 and 35% w/v 2-methyl-2,4- pentanediol 100mM Imidazole, pH 8.0 have been identified as suitable for crystallization of chNet△C- Neo Long 3-5 complex and chNet△C- Neo Short 3-5 complex, respectively. However, further optimization of these conditions is necessary and there is an ongoing attempt to crystallize the complex.

6. References

(1) Llambi, F., Causeret, F., Bloch-Gallego, E., & Mehlen, P. (2001). Netrin-1 acts as a survival factor via its receptors UNC5H and DCC. *EMBO Journal*, *20*(11), 2715–2722. https://doi.org/10.1093/emboj/20.11.2715

(2) *Kennedy TE, Serafini T, de la Torre JR and Tessier-Lavigne M (1994) Netrins are diffusible chemotropic factors for commissural axons in the embryonic spinal cord. Cell, 78, 425–435.*

(3) *Colamarino SA and Tessier-Lavigne M (1995) The axonal chemoattractant netrin-1 is also a chemorepellent for trochlear motor axons. Cell, 81, 621–629.*

(4) Grandin, M. (2018). Structural Decoding of the Netrin-1/UNC5 Interaction and its Therapeutical Implications in Cancers. *Cancer Cell*, *29*(2), 173–185. https://doi.org/10.1016/j.ccell.2016.01.001

(5) Raphael Reuten, Trushar R. Patel, Matthew Mcdougall, Nicolas Rama, Denise Nikodemus, Benjamin Gibert, … Manuel Koch. (2016). Structural decoding of netrin-4 reveals a regulatory function towards mature basement membranes. *Nature Communications*, *7*, 13515. https://doi.org/10.1038/ncomms13515

(6) Bhama Ramkhelawon, Elizabeth J Hennessy, Mickaël Ménager, Tathagat Dutta Ray, Frederick J Sheedy, Susan Hutchison, … Kathryn J Moore. (2014). Netrin-1 promotes adipose tissue macrophage retention and insulin resistance in obesity. *Nature Medicine*, *20*(4), 377–384. https://doi.org/10.1038/nm.3467

(7) Bongo, J., & Peng, D. (2014). The neuroimmune guidance cue netrin-1: A new therapeutic target in cardiovascular disease. *Journal of Cardiology*. Elsevier Ltd. https://doi.org/10.1016/j.jjcc.2013.10.006

(8) Ylivinkka, I., Keski-Oja, J., & Hyytiäinen, M. (2016). Netrin-1: A regulator of cancer cell motility? *European Journal of Cell Biology*, *95*(11), 513–520. https://doi.org/10.1016/j.ejcb.2016.10.002

(9) Geisbrecht, B., Dowd, K., Barfield, R., Longo, P., & Leahy, D. (2003). Netrin binds discrete subdomains of DCC and UNC5 and mediates interactions between DCC and heparin. *Journal of Biological Chemistry*, *278*(35), 32561–32568. https://doi.org/10.1074/jbc.M302943200

(10) Delloye-Bourgeois, C., Fitamant, J., Paradisi, A., Cappellen, D., Douc-Rasy, S., Raquin, M., … Mehlen, P. (2009). Netrin-1 acts as a survival factor for aggressive neuroblastoma. *The Journal of Experimental Medicine*, *206*(4), 833–847. https://doi.org/10.1084/jem.20082299

(11) Xu, K., Wu, Z., Renier, N., Antipenko, A., Tzvetkova-Robev, D., Xu, Y., … Nikolov, D. (2014). Neural migration. Structures of netrin-1 bound to two receptors provide insight into its axon guidance mechanism. *Science (New York, N.Y.)*, *344*(6189), 1275–1279. https://doi.org/10.1126/science.1255149

(12) Mehlen, P., & Thibert, C. (2004). Dependence receptors: between life and death. *Cellular and Molecular Life Sciences*, *61*(15), 1854–1866. https://doi.org/10.1007/s00018-004-3467-7

(13)Serafini, T., Colamarino, S., Leonardo, E., Wang, H., Beddington, R., Skarnes, W., & Tessier-Lavigne, M. (1996). Netrin-1 Is Required for Commissural Axon Guidance in the Developing Vertebrate Nervous System. *Cell*, *87*(6), 1001–1014. https://doi.org/10.1016/S0092-8674(00)81795-X

(14)F Mille, F Llambi, C Guix, C Delloye-Bourgeois, C Guenebeaud, S Castro-Obregon, … P Mehlen. (2009). Interfering with multimerization of netrin-1 receptors triggers tumor cell death. *Cell Death and Differentiation*, *16*(10), 1344–1351. https://doi.org/10.1038/cdd.2009.75

(15) Kruger, R., Lee, J., Li, W., & Guan, K. (2004). Mapping netrin receptor binding reveals domains of Unc5 regulating its tyrosine phosphorylation. *The Journal of Neuroscience : the Official Journal of the Society for Neuroscience*, *24*(48), 10826–10834. https://doi.org/10.1523/JNEUROSCI.3715-04.2004

(16) SanGiovanni, J., Chen, J., Gupta, A., Smith, L., Sapieha, P., & Lee, P. (2015). Netrin-1 – DCC Signaling Systems and Age-Related Macular Degeneration. *PLoS ONE*, *10*(5), e0125548. https://doi.org/10.1371/journal.pone.0125548

(17) Fothergill, T., Donahoo, A., Douglass, A., Zalucki, O., Yuan, J., Shu, T., … Richards, L. (2014). Netrin-DCC Signaling Regulates Corpus Callosum Formation Through Attraction of Pioneering Axons and by Modulating Slit2-Mediated Repulsion. *Cerebral Cortex*, *24*(5), 1138–1151. https://doi.org/10.1093/cercor/bhs395

(18) Goldschneider, D., & Mehlen, P. (2010). Dependence receptors: a new paradigm in cell signaling and cancer therapy. *Oncogene*, *29*(13), 1865–1882. https://doi.org/10.1038/onc.2010.13

(19) Moore, S., Kennedy T., Tessier-Lavigne M. (2009) Axonal Pathfinding: Netrins. *Encylopedia of Neuroscience,* 1155-1162. https://doi.org/10.1016/B978-008045046-9.00333-8

(20)Tsuchiya, A., Hayashi, T., Deguchi, K., Sehara, Y., Yamashita, T., Zhang, H., … Abe, K. (2007). Expression of netrin-1 and its receptors DCC and neogenin in rat brain after ischemia. *Brain Research*, *1159*, 1–7.

(21) Jae Ho Lee, Sung Sook Choi, Hae-Won Kim, Wen Cheng Xiong, Churl K Min, & Sang Jin Lee. (2014). Neogenin as a receptor for early cell fate determination in preimplantation mouse embryos. *PLoS ONE*, *9*(7), e101989. https://doi.org/10.1371/journal.pone.0101989

(22) O' Leary, C., Bradford, D., Chen, M., White, A., Blackmore, D., & Cooper, H. (2015). The Netrin/RGM Receptor, Neogenin, Controls Adult Neurogenesis by Promoting Neuroblast Migration and Cell Cycle Exit. *STEM CELLS*, *33*(2), 503–514. https://doi.org/10.1002/stem.1861

(23)König, K., Gatidou, D., Granja, T., Meier, J., Rosenberger, P., Mirakaj, V., & Eltzschig, H. (2012). The Axonal Guidance Receptor Neogenin Promotes Acute Inflammation (Neogenin and Inflammation). *PLoS ONE*, *7*(3), e32145. https://doi.org/10.1371/journal.pone.0032145

(24) Hagihara, M., Endo, M., Hata, K., Higuchi, C., Takaoka, K., Yoshikawa, H., … Hagihara, M. (2011). Neogenin, a receptor for bone morphogenetic proteins. *The Journal of Biological Chemistry*, *286*(7), 5157–5165. https://doi.org/10.1074/jbc.M110.180919

(25) Wang, H., Copeland, N., Gilbert, D., Jenkins, N., Tessier-Lavigne, M., & Wang, H. (1999). Netrin-3, a Mouse Homolog of Human NTN2L, Is Highly Expressed in Sensory Ganglia and Shows Differential Binding to Netrin Receptors. *Journal of Neuroscience*, *19*(12), 4938–4947. https://doi.org/10.1523/JNEUROSCI.19-12-04938.1999

(26) Wilson, N., & Key, B. (2006). Neogenin interacts with RGMa and Netrin-1 to guide axons within the embryonic vertebrate forebrain. *Developmental Biology*, *296*(2), 485–498. https://doi.org/10.1016/j.ydbio.2006.06.018

(27) Srikanth Rajagopalan, Lutz Deitinghoff, Denise Davis, Sabine Conrad, Thomas Skutella, Alain Chedotal, … Stephen M. Strittmatter. (2004). Neogenin mediates the action of repulsive guidance molecule. *Nature Cell Biology*, *6*(8), 756–762. https://doi.org/10.1038/ncb1156

(28) Qu, H. (2018). Neogenin-1 Promotes Cell Proliferation, Motility, and Adhesion by Up-Regulation of Zinc Finger E-Box Binding Homeobox 1 Via Activating the Rac1/PI3K/AKT Pathway in Gastric Cancer Cells. *Cellular Physiology and Biochemistry*, *48*(4), 1457–1467. https://doi.org/10.1159/000492255

(28) Huang, X., Wilber, A., Bao, L., Tuong, D., Tolar, J., Orchard, P., … Zhou, X. (2006). Stable gene transfer and expression in human primary T cells by the Sleeping Beauty transposon system. *Blood*, *107*(2), 483–491. https://doi.org/10.1182/blood-2005-05-2133

(29) Qin, J., Zhang, L., Clift, K., Hulur, I., Xiang, A., Ren, B., … Hansen, I. (2010). Systematic Comparison of Constitutive Promoters and the Doxycycline-Inducible Promoter (Comparison of Promoters). *PLoS ONE*, *5*(5), e10611. https://doi.org/10.1371/journal.pone.0010611

(30) Wang, Y., Ye, Z., & Ying, Y. (2013). Detection of immunoglobulin E using an aptamer based dot-blot assay. *Chinese Science Bulletin*, *58*(24), 2938–2943. https://doi.org/10.1007/s11434-013-5702-9

(31) Kearney, B., Voorhees, M., Williams, P., Olschner, S., Rossi, C., & Schoepp, R. (2017). Corning HYPERFlask® for viral amplification and production of diagnostic reagents. *Journal of Virological Methods*, *242*, 9–13. https://doi.org/10.1016/j.jviromet.2016.12.011

(32) Gasteiger E., Hoogland C., Gattiker A., Duvaud S., Wilkins M.R., Appel R.D., Bairoch A.; *Protein Identification and Analysis Tools on the ExPASy Server;*
(In) John M. Walker (ed): The Proteomics Protocols Handbook, Humana Press (2005).
pp. 571-607

(33) Tuukkanen, A., Spilotros, A., Svergun, D., & Tuukkanen, A. (2017). Progress in small-angle scattering from biological solutions at high-brilliance synchrotrons. *IUCrJ*, *4*(Pt 5), 518–528. https://doi.org/10.1107/S2052252517008740

(34) Murthy, N. (2017). Recent Developments in Small-Angle X-Ray Scattering. *Spectroscopy*, *32*(s11), 18–24. Retrieved from http://search.proquest.com/docview/1966003784/

(35) Petoukhov, M., Svergun, D., & Petoukhov, M. (2013). Applications of small-angle X-ray scattering to biomacromolecular solutions. *The International Journal of Biochemistry & Cell Biology*, *45*(2), 429–437. https://doi.org/10.1016/j.biocel.2012.10.017

(36)Putnam, C., Hammel, M., Hura, G., & Tainer, J. (2007). X-ray solution scattering (SAXS) combined with crystallography and computation: defining accurate macromolecular structures, conformations and assemblies in solution. *Quarterly Reviews of Biophysics*, *40*(3), 191–285. https://doi.org/10.1017/S0033583507004635

(37) Ruseva, V., Lyons, M., Powell, J., Austin, J., Malm, A., & Corbett, J. (2018). Capillary dynamic light scattering: Continuous hydrodynamic particle size from the nano to the micro-scale. *Colloids and Surfaces A: Physicochemical and Engineering Aspects*, *558*, 504–511. https://doi.org/10.1016/j.colsurfa.2018.09.022

(38) Schaff, F., Bech, M., Zaslansky, P., Jud, C., Liebi, M., Guizar-Sicairos, M., … Schaff, F. (2015). Six-dimensional real and reciprocal space small-angle X-ray scattering tomography. *Nature*, *527*(7578), 353–356. https://doi.org/10.1038/nature16060

(39) Liu, H., & Zwart, P. (2012). Determining pair distance distribution function from SAXS data using parametric functionals. *Journal of Structural Biology*, *180*(1), 226–234. https://doi.org/10.1016/j.jsb.2012.05.011

(40) Grant, T. (2018). Ab initio electron density determination directly from solution scattering data.(Report). *Nature Methods*, *15*(3), 191–193. https://doi.org/10.1038/nmeth.4581

(41) Koutsioubas, A., & Perez, J. (2013). Incorporation of a hydration layer in the `dummy atom' ab initio structural modelling of biological macromolecules. *Journal of Applied Crystallography*, *46*(6), 1884–1888. https://doi.org/10.1107/S0021889813025387

(42) Hou, H., Shi, M., Hu, S., Ahmad, F., Zhang, B., Chen, Z., & Yin, D. (2019). A systematic comparison of sitting and hanging-drop crystallization using traditional and cross-diffusion microbatch crystallization plates. *Journal of Crystal Growth*, *521*, 1–8. https://doi.org/10.1016/j.jcrysgro.2019.05.011

7. Appendix

7.1 LIST OF ABBREVIATIONS

χ	Chi Value
ASN	Amino Acid Asparagine
DAG	Diacylglycerol
DCC	Deleted in Colorectal Cancer
DENSS	Density from Solution Scattering
DLS	Dynamic Light Scattering
D_{max}	Maximum particle dimension
DMEM	Dulbecco's Modified Eagle Medium
DMSO	Dimethyl Sulfoxide
DNA	Deoxyribonucleic Acid
EDTA	Ethylenediaminetetraacetic acid
FAK	Focal Adhesion Kinase
FBS	Fetal Bovine Serum
CO_2	Carbon Dioxide
FN	Fibronectin Type Domains
FYN	Tyrosine Protein Kinase
GPI	Glycosylphosphatidylinositol
HABA	4'-hydroxyazobenzene-2-carboxylic acid
HEK	Human Embryonic Kidney
HRP	Horseradish Peroxide
IG	Immunoglobulin Domains
IP3	Inositol 1,3,5- triphosphate
LE	Laminin-type epidermal growth factors
LN	Laminin Domain
MAP	Microtubule Associated Proteins
MAPK	Mitogen-activated protein kinases
NEO	Neogenin
NTN1	Netrin-1 Gene
P(r)	Electron pair distribution function
PAK	Threonine Protein Kinase
PEG	Polyethylene Glycol
PI3K	Phosphoinositide 3-kinases
PIPs	Phosphoinositides

PITPα	Phosphatidylinositol transfer protein- α
PKC	Protein Kinase C
PLC	Phospholipase C
RAC	Ras Related Protein
R_g	Radius of Gyration
RGMa	Repulsive Guidance Molecule a
R_H	Radius of Hydration
SAXS	Small angle X-ray scattering
SDS PAGE	Sodium dodecyl sulfate polyacrylamide gel electrophoresis
SEC	Size exclusion chromatography
TRE	Tetracycline Inducible Expression
UNC5	Uncoordinated 5
VASP	Vasodilator-stimulated phosphoprotein